LOW-FREQUENCY LINEAR VIBRATIONS OF SINGLE-WALLED CARBON NANOTUBES: ANALYTICAL AND NUMERICAL MODELS

Matteo Strozzi*, Leonid I. Manevitch°, Francesco Pellicano*,
Valeri V. Smirnov°, Denis S. Shepelev°

*Department of Engineering "Enzo Ferrari"
University of Modena and Reggio Emilia
Via Vignolese 905, 41125 Modena, Italy

°N.N. Semenov Institute of Chemical Physics
Russian Academy of Sciences RAS
ul. Kosygina 4, 119991 Moscow, Russia

Running headline: Low-Frequency Linear Vibrations of Single-Walled Carbon Nanotubes: Analytical and Numerical Models

Number of Pages = 56
Number of Tables = 9
Number of Figures = 9

Dr. Francesco Pellicano, Professor
Department of Engineering "Enzo Ferrari"
University of Modena and Reggio Emilia
Strada Vignolese 905
41121 Modena, Italy
Ph: +39 059 205 6154
Fax: +39 059 205 6126
email: francesco.pellicano@unimore.it

Abstract

Low-frequency vibrations of Single-Walled Carbon Nanotubes with various boundary conditions are considered in the framework of the Sanders-Koiter thin shell theory. Two methods of analysis are proposed. The first approach is based on the Rayleigh-Ritz method, a double series expansion in terms of Chebyshev polynomials and harmonic functions is considered for the displacement fields; free and clamped edges are analysed. This approach is partially numerical. The second approach is based on the same thin shell theory, but the goal is to obtain an analytical solution useful for future developments in nonlinear fields; the Sanders-Koiter equations are strongly simplified neglecting in-plane circumferential normal strains and tangential shear strains. The model is fully validated by means of comparisons with experiments, molecular dynamics data and finite element analyses obtained from the literature. Several types of nanotubes are considered in detail by varying aspect ratio, chirality and boundary conditions. The analyses are carried out for a wide range of frequency spectrum. Strength and weakness of the proposed approaches are shown; in particular, the model shows great accuracy even though it requires minimal computational effort.

Keywords

Single-Walled Carbon Nanotubes; Linear vibrations; Continuous thin shell models

1. Introduction

Carbon Nanotubes were discovered in 1991 by Iijima [1], who first analysed the synthesis of molecular carbon structures in the form of fullerenes and then reported the preparation of a new type of finite carbon structure consisting of needle-like tubes, the carbon nanotubes, described as helical microtubules of graphitic carbon.

Carbon Nanotubes (CNTs) are used as ultrahigh frequency nanomechanical resonators in a large number of nanoelectromechanical devices such as sensors, oscillators, charge detectors and field emission devices. The reduction of the size and the increment of the stiffness of a resonator magnify its resonant frequencies and reduce its energy consumption, improving its sensitivity.

The modal analysis of carbon nanotubes is important because it allows to obtain the resonant frequencies and mode shapes, which influence the mechanical and electronic properties of the nanotube resonators.

A large number of experiments and atomistic simulations were conducted both on single-walled (SWNTs) and multi-walled carbon nanotubes (MWNTs).

Rao et al. [2] studied the vibrations of SWNTs by using Raman scattering experimental techniques with laser excitation wavelengths in the range of the nanometers. They observed numerous Raman peaks, which correspond to vibrational modes of the nanotubes.

Bandow et al. [3] analysed the effect of the temperature growth on the diameter distribution and chirality of SWNTs by comparing different experimental techniques, such as electron microscopy, X-ray diffraction and Raman spectroscopy. They studied the effect of the catalysts on the tube yield and the evolution of the tube distribution vs. the environmental temperature.

Jorio et al. [4] studied the vibrations of SWNTs by resonant confocal micro-Raman spectroscopy. They developed a method to assign univocally the carbon nanotube chirality by measuring one radial breathing mode frequency and applying the theory of resonant transitions.

Because of their nanoscale size, it is very difficult to investigate the mechanical properties of the nanotubes using experimental techniques, which require the use of high resolution transmission electron microscopes and do not allow to separate easily the natural frequencies of the different vibration modes within the frequency spectrum. On the other hand, it was found that molecular dynamics simulations (MD) and finite element analyses (FE) provide good predictions of the mechanical behaviour of CNTs under external forces, with results close to the experiments.

Gupta et al. [5] analysed the free vibrations of zigzag SWNTs using molecular mechanics (MM) simulations with the MM3 potential, taking into account the effect of transverse inertia forces. They computed natural frequencies of inextensional Rayleigh-Love modes and radial breathing modes by considering different aspect ratios and chiralities.

Cheng et al. [6] investigated the radial breathing mode frequencies (RBM) and mode shapes of carbon nanotubes using a modified molecular structural mechanics model (MSM). They considered CNTs with different geometries and configurations, taking into account also the effect of the temperature.

Gupta et al. [7] simulated the mechanical behaviour of SWNTs with free edges by using the MM3 potential (MD model). They considered the effect of the chirality and the geometry on the natural frequencies of the longitudinal, torsional and inextensional modes of vibration of the nanotubes.

Duan et al. [8] studied the free vibrations of carbon nanotubes by MD simulations considering clamped-free and free-free boundary conditions, with different aspect ratios and mode shapes. They introduced the concept of nonlocal scaling effect parameter.

Sakhaee-Pour et al. [9] performed a vibration analysis of SWNTs using an FE method based on beam elements. The vibrational behaviour of clamped-clamped and clamped-free carbon nanotubes with different aspect ratios was modelled by using three-dimensional elastic beams and point masses, considering covalent bonds between the carbon atoms in the hexagonal lattice of the atomic structure.

Arghavan and Singh [10] carried out a numerical study on the free and forced vibrations of SWNTs by considering the standard FE method (frame model). They analysed different chiralities for clamped-clamped and clamped-free boundary conditions, obtaining natural frequencies and corresponding mode shapes, and reported time histories and spectra of the axial, bending and torsional modes of vibration.

However, it has been demonstrated that MD simulations and FE analyses are computationally inefficient, especially when dealing with multi-walled CNTs incorporating a large number of atoms; for the same reason, such models are not well suited for including nonlinear effects. Therefore, more efficient analytical and numerical methods have been recently developed in order to analyse classes of CNTs in a more general and efficient way; such methods are generally based on continuous models for the nanotube and allow a strong reduction of the number of degrees of freedom.

Notwithstanding their small size and a discrete nature, CNTs were found to behave similarly to thin walled continua having both membrane and bending stiffness; therefore, it became evident that the equivalent continuous models could represent a very efficient way for the analysis and prediction of the carbon nanotubes behaviour.

Odegard et al. [11] proposed an equivalent continuous model of nano-structured materials in which a representative volume element of graphene chemical structure was substituted with an equivalent continuous cylinder; they determined the effective thickness and bending rigidity of graphene.

Lu et al. [12] applied nonlocal Euler and Timoshenko beam models in order to investigate the vibration properties of single-walled and multi-walled CNTs. They derived the equations of motion for the different nonlocal beam models and analysed the influence of nonlocal effects on the wave properties, i.e., natural frequencies and phase velocities.

Yang et al. [13] developed an efficient multiscale model for the CNTs by assuming the molecular structure equivalent to a solid cylinder. They analysed the effect of the size on the effective elastic stiffness of CNT/polymer nano-composites with interfacial imperfections.

Kiani [14] developed a meshless approach for the analysis of the free transverse vibrations of a single-walled carbon nanotube embedded in an elastic matrix. Arbitrary boundary conditions were considered. The discrete equations of motion were established in the context of nonlocal continuum mechanics of Eringen, using the Hamilton's principle and an efficient meshless method. The nonlocal effect was taken into account. In Refs. [15-16] the same author applied Rayleigh, Timoshenko and higher-order nonlocal beam theories to study the vibration characteristics of double-walled carbon nanotubes under a moving nanoparticle. The effects of slenderness ratio and small scale parameter were investigated for different boundary conditions. Theoretical formulations were reported, a parametric study was developed. Ref. [17] analysed the free transverse vibrations of a double-walled carbon nanotube embedded in an elastic foundation subjected to an initial axial load. Rayleigh, Timoshenko and higher-order nonlocal beam theories were used. The influence of the small-scale parameter, initial axial force, lateral and rotational stiffness of the surrounding matrix on the flexural frequencies was examined for different boundary conditions. The same author [18] analyzed the vibrational behavior of simply supported inclined single-walled carbon nanotubes conveying viscous fluids flow using the nonlocal Rayleigh beam model. The equations of motion were obtained in the context of nonlocal elasticity theory of Eringen. The effects of the small-scale parameter, inclination angle, speed and density of the fluid flow were considered.

Wang and Hu [19] studied the flexural wave propagation in a SWNT comparing the results of the traditional Timoshenko beam theory and the nonlocal Timoshenko beam theory with the molecular dynamics simulations based on the Tersoff-Brenner potential. They found that the microstructure of a nanotube has a significant influence on the dispersion of flexural waves only for high frequencies.

Fazelzadeh and Ghavanloo [20] developed a nonlocal anisotropic elastic shell model to study the effect of small scale on the vibrations of SWNTs with arbitrary chirality. They found that the effect of nonlocal parameters on the frequency is significant only for the SWNTs with low aspect ratios and small diameters.

In particular, it was found that the continuous shell model can predict the static buckling and free vibrations behaviours obtained with the atomistic molecular-dynamics simulations: the analogies

between the elastic shell model and the CNTs structure led to an extensive application of the shell model for the CNTs structural analysis.

Ru [21] studied the buckling effect of a double-walled carbon nanotube embedded in an elastic medium under axial compression by considering an elastic double-shell model. He applied the Donnell shallow shell theory and modelled the interaction between the inner and outer nanotubes by considering the Van der Waals forces.

Eisenberger et al. [22] analysed the effect of the Van der Waals interactions on the vibration characteristics of multi-walled carbon nanotubes. An elastic multiple thin shell model was used. Based on the simplified Donnell shell equations, the natural frequencies and mode shapes of MWNTs with various radii and number of tubes were obtained.

Elishakoff and Pentaras [23] evaluated the fundamental natural frequencies of double-walled carbon nanotubes under various boundary conditions with the Donnell shallow shell theory. They applied the Bubnov-Galerkin and Petrov-Galerkin approximate methods to derive explicit expressions for the natural frequencies.

Silvestre et al. [24] studied the buckling behaviour of SWNTs with small aspect ratios comparing the Donnell shallow shell and Sanders-Koiter thin shell theories. They demonstrated the inability of the Donnell shallow shell theory and the validity of the Sanders-Koiter shell theory in reproducing buckling strains and mode shapes of axially compressed CNTs very close to the MD ones. Simply supported and clamped-clamped boundary conditions were considered.

Peng et al. [25] quantified the error in approximating SWCNTs as continuous thin shells via an atomistic-based finite-deformation shell theory. They found that SWCNTs with small diameters cannot be represented by a conventional elastic thin shell because their constitutive relation involves the coupling between tension and curvature and between bending and strain due to non-local effects.

In order to analyse the discrete molecular carbon nanotubes as continuum thin shells, different equivalent mechanical and geometric parameters have been proposed.

Huang et al. [26] determined the equivalent values of the wall thickness and Young's modulus of SWNTs by considering the expressions of the tension and bending rigidities obtained directly from the interatomic potential of graphene.

Yao and Lordi [27] used MD simulations in order to calculate the equivalent Young's modulus of Single-Walled Carbon Nanotubes with different geometries from their thermal vibration frequencies and torsional strains.

Yakobson et al. [28] studied the instabilities beyond linear response of carbon nanotubes subjected to large deformations. With properly chosen tubule equivalent Poisson's ratio, Young's modulus

and wall thickness, they determined the critical buckling values of the carbon nanotube under axial, bending and torsional strains.

Jin and Yuan [29] obtained the equivalent value of the elastic modulus of Single-Walled Carbon Nanotubes subjected to small-strain deformation by using Molecular Dynamics simulations with both energy and force approaches.

Vodenitcharova and Zhang [30] investigated the equivalent wall thickness and Young's modulus of a SWNT by considering the deformation of a bundle of Single-Walled Carbon Nanotubes subjected to an external hydrostatic pressure and using the continuum mechanics theory.

Different elastic shell theories have been applied in order to study the mechanical behaviour of Single-Walled Carbon Nanotubes as continuum structures.

Liew and Wang [31] investigated the wave propagation in both SWNTs and DWNTs by comparing two different elastic shell theories: the Love's thin cylindrical shell theory and the Cooper-Naghdi thick cylindrical shell theory, where in the second theory the shear and inertia effects are taken into account in order to provide more accurate wave dispersions for the higher vibration modes.

Carrera and Brischetto [32] compared two classical two-dimensional models, such as Classical Lamination Theory (CLT) and First order Shear Deformation Theory (FSDT), and a refined mixed model based on Carrera Unified Formulation (CUF) for the analysis of nano-reinforced structures. Several types of nanocomposites were used in the static analysis of the circular cylindrical shells, their elastic properties have been obtained from an accurate literature review.

Silvestre [33] evaluated the accuracy of different shell models for the torsional buckling of SWNTs. He found that the Donnell shallow shell model leads to incorrect values of the critical angle of twist per unit length compared with the MD results. Conversely, he proved that the Sanders shell model leads to correct results of the critical angle of twist.

Wang et al. [34] examined the applicability and limitations of different simplified models of elastic cylindrical shells for general cases of static buckling and free vibrations of carbon nanotubes. They found that the simplified Flugge model, which retains the mathematical simplicity of the Donnell model, is in better agreement with the Flugge equations with respect to the Donnell theory.

Cong [35] determined the critical buckling strains of SWNTs subjected to axial compression by using different cylindrical shell theories. Considering MD simulations as benchmarks, he found that the first-order shear deformation thick shell theory gives a closer prediction of the critical buckling strains when compared with the Donnell and the Sanders elastic thin shell theories.

In the pertinent literature, the SWNTs are frequently modelled as isotropic elastic thin shells.

On the other hand, Ghavanloo and Fazelzadeh [36] studied the linear vibrations of the SWNTs by considering an anisotropic model based on the Flugge elastic shell theory including the chirality

effect. They analysed the effect of the tube chirality on the natural frequencies of the CNTs and the influence of externally applied mid-face axial force and torque on the frequencies of chiral SWNTs. Chang [37] developed a molecular mechanics based anisotropic elastic shell model for studying the mechanical behaviour of SWNTs. He analysed the effects of the size and chirality on: the coupling between axial, circumferential and torsional deformations; the radial breathing mode frequency; the longitudinal and torsional wave propagation speeds.

Readers interested in deepening the knowledge on shells behaviour are suggested to refer to the works of Leissa [38] and Yamaki [39]. The first one is mainly concerned with the linear dynamics of shells exhibiting different topologies, materials and boundary conditions. The second one is focused on buckling and post-buckling of the shells in linear and nonlinear fields. In Refs. [38,39] one can find the most important shell theories, such as Donnell, Reissner, Flugge, Sanders-Koiter, as well as solution methods, numerical and experimental results. In Ref. [40] the nonlinear vibrations and stability of circular cylindrical shells are analysed. Refs. [41-44] are strictly related to the present work. In Refs. [41,42] a method based on the nonlinear Sanders-Koiter theory and a displacement expansion based on Chebyshev polynomials and harmonic functions was presented; moreover, in Ref. [43] the same method was applied to Functionally Graded shells and extended to several types of boundary conditions, e.g., free-free, which are of great interest for the present study. In Ref. [44] a reduced shell theory was proposed, the expression of the elastic strain energy neglects the circumferential and tangential shear deformations; this model is the basis for the reduced version of the Sanders-Koiter theory proposed in the present work.

In the present paper, we analyse the low-frequency linear vibrations of SWNTs by using two shell models. Applicability and limitations of these continuous models are investigated in detail.

The first approach is semi-analytical and it is based on the Rayleigh-Ritz numerical procedure, we call it shortly “numerical approach”; the Sanders-Koiter shell theory is considered in order to obtain the expressions of the elastic strain and kinetic energy. The nanotube deformation is described in terms of longitudinal, circumferential and radial displacement fields, which are expanded by means of a double mixed series based on Chebyshev polynomials for the longitudinal variable and harmonic functions for the circumferential variable. The Rayleigh-Ritz method is then applied to obtain numerically approximate natural frequencies and mode shapes.

The second approach consists of an analytical model based on a reduced version of the Sanders-Koiter shell theory, obtained by assuming small ring and tangential shear deformations. These assumptions allow to condense both the longitudinal and the circumferential displacement fields. A fourth-order partial differential equation for the radial displacement field is derived. Eigenfunctions

are formally obtained analytically, then the numerical solution of the dispersion equation gives the natural frequencies and the corresponding normal modes.

In order to validate the present study, the natural frequencies of the carbon nanotube predicted by the present numerical model are compared with data available in literature: experiments, molecular dynamics simulations and finite element analyses. A comparison between the results of the numerical and analytical approach is carried out in order to check the accuracy of the last one. It is worthwhile to stress that the analytical model allows to obtain results with very low computational effort.

2. Applicability and limitations of continuous thin shell models for Carbon Nanotubes

In the study of the mechanical behaviour of CNTs by means of elastic thin shell models, three different problems must be taken into account.

The first issue concerns the definition of the equivalent mechanical and geometric parameters of the shell model; the nanotube can be considered as a graphene sheet rolled into a seamless tube; its behaviour can be modelled through a thin cylindrical shell theory, where the equivalent values of Young's modulus E, Poisson's ratio ν and wall thickness h must be properly set.

The second issue is related to the particular elastic shell theory to be applied for the computation of the elastic strain energy of the carbon nanotube: the results obtained using different shell theories (Flugge, Donnell, Sanders-Koiter, first-order shear deformation) should be compared with available MD simulations and experimental observations.

The third issue concerns the methods of solution of the linear or nonlinear partial differential equations that govern the shell mechanics; such methods must be accurate but also as simple as possible and computationally efficient. Indeed, shell theories are used to replace MD models, which are the most coherent with the nanotube structure, but they are computationally inefficient; therefore, shell theories and solution methods must exhibit higher efficiency and, possibly, they should allow analytic or semi-analytic solutions.

The literature deeply analysed the first two issues, it appears that shell models based on refined theories like Donnell-Mushtari or Sanders-Koiter are quite accurate using equivalent parameters. Regarding the solution methods some aspects are open in the literature: i) often only simply supported boundary conditions are considered, as they allow simple analytical-numerical treatments; ii) several approaches are not suitable for extension to nonlinear field, which is the future step for understanding complex CNT behaviours.

2.1. Equivalent parameters

Since the elastic properties of a two-dimensional hexagonal structure are isotropic, the graphene sheet rolled into a seamless tube can be approximated as a shell by using three different elastic parameters, i.e., tensile rigidity C, bending rigidity D and Poisson's ratio ν [26].

Experimental observations have shown that CNTs have effective Young's modulus $E_0 = 1.0 \div 2.0$ TPa, Poisson's ratio $\nu_0 = 0.12 \div 0.28$ and wall thickness $h_0 = 0.10 \div 0.15$ nm, even if it is ambiguous to define the thickness of a single layer of atoms, as it is pointed out in the modelling proposed in Ref. [27].

The parameters C and D were identified by comparisons with MD simulations of the CNTs energy, in Ref. [28] the following parameters are reported: $C = 59$ eV / atom $= 360$ J / m^2 and $D = 0.85$ eV

= 1.362 × 10^{-19} J, while the equivalent Poisson's ratio ν = 0.19 was extracted from a reduction of the diameter of a tube stretched in simulations at small strains.

It should be pointed out that effective parameters are referred to the equivalent continuous models of the bar/beam, i.e., models that consider the full cross section area of the tube.

In the modelling of a SWNT as a continuum elastic thin shell, the equivalent Young's modulus E and wall thickness h can be determined by using the standard relations of the tensile rigidity C and bending rigidity D from the classical shell theory, in the following form [28]

$$C = Eh \qquad D = \frac{Eh^3}{12(1-\nu^2)} \tag{1}$$

Such an approach gives an equivalent thickness h = 0.066 nm and Young's modulus E = 5.5 TPa.

It is important to point out that the equivalent wall thickness h = 0.066 nm is much smaller than the graphite interlayer spacing h = 0.340 nm: when this representative wall thickness (planar spacing of graphite) is considered together with a representative Young's modulus equal to E = 1.06 TPa (bulk stiffness of graphite) in the standard relations of the classical shell theory, the tensile rigidity C is similar to the MD results, while the bending rigidity D is much greater than the one obtained from atomistic simulations; therefore, the results obtained with the representative parameters are different from those obtained by using MD simulations [30]. This paradox justifies the use of the equivalent shell parameters previously identified for C and D.

In the present work, the equivalent parameters E = 5.5 TPa, ν = 0.19, h = 0.066 nm are considered in order to model the discrete SWTN using an equivalent continuum elastic thin shell theory, with a surface density of graphite σ = 7.718 × 10^{-7} kg/m^2 and a mass density ρ = 11700 kg/m^3 as calculated by the relation $\rho = \sigma / h$, with h = 0.066 nm. Note that the equivalent Young's modulus is higher than the effective one; indeed, it must be considered that in the shell model the cross section area depends on the radius and the shell thickness.

It is worthwhile to stress that the aforementioned elastic parameters E, ν, ρ, h have been found suitable for equivalent thin shell models. If one simulates the nanotube by using e.g. a beam frame, then different equivalent parameters must be considered.

2.2. Elastic shell theories

Different elastic shell theories have been applied in the past in order to study the mechanical behaviour of SWNTs as continuum systems.

Elastic thin shell theories, such as Donnell-Mushtari, Donnell shallow shell and Sanders-Koiter, are based on the following assumptions, i.e., the Love's "first approximation" [38]: 1) the thickness of the shell is small compared with the radius and the shell is sufficiently thin, i.e., $h / R < 0.05$; 2) the strains and the displacements are sufficiently small so that the quantities of the second and higher-order magnitude in the strain-displacement relations may be neglected in comparison with the first-order terms; 3) the transverse normal stress is small compared with the other normal stress components and may be neglected; 4) the normal to the undeformed middle surface remains straight and normal to the deformed middle surface and it suffers no extension; 5) the rotary inertia and transverse shear deformation effects may be neglected.

Donnell shallow shell equations are widely used in the literature both in nano and in macro scales; in any case the limitations of this theory must be carefully considered, the main simplification is the static condensation of the in-plane inertia, which leads to severe inaccuracies for modes having a number of nodal diameters between 1 and 4 (non-breathing modes); other limitations regard the kinematic description of the strain-displacement relationships, see Ref. [38] for deepen the topic and [33] for a specific application to CNTs.

Ref. [34] reports interesting comparisons between Donnell, Flugge and simplified Flugge theories regarding the static buckling under axial compression and radial pressure of CNTs; additionally, in this paper an extremely simplified version of the Flugge equations, specialized for radial breathing modes only, was presented.

In Ref. [35] a higher-order shear deformation model, based on the Reddy theory, was used in order to improve the results of the thin shell theories in the analysis of CNTs.

Carbon Nanotubes are often modelled as isotropic elastic cylindrical shells. The anisotropies due to the intrinsic discrete nature of CNTs can be neglected because they give a marginal contribution.

In this work, SWNTs are modelled as isotropic elastic thin shells [41]; two independent mechanical properties, i.e., elastic modulus and Poisson's ratio, are considered. The Sanders-Koiter shell theory is applied to study the vibrations of SWNTs considering the most important types of boundary conditions.

Considering the plane stress approximation ($\sigma_z = 0$), the stresses (σ_x, σ_θ, $\tau_{x\theta}$) are related to the strains (ε_x, ε_θ, $\gamma_{x\theta}$) by the following relationships [41]

$$\sigma_x = \frac{E}{1-\nu^2}(\varepsilon_x + \nu\varepsilon_\theta) \qquad \sigma_\theta = \frac{E}{1-\nu^2}(\varepsilon_\theta + \nu\varepsilon_x) \qquad \tau_{x\theta} = \frac{E}{2(1+\nu)}\gamma_{x\theta} \tag{2}$$

where E is the Young's modulus and ν is the Poisson's ratio.

A very important issue concerns the inclusion of the size effects into the elastic shell theory used to model SWNTs as continuum systems. Nanostructures can behave differently from macrostructures due to the presence of significant size effects that are not present at a macro scale, i.e., surface stresses, strain gradients and non-locality [14-18]. Since the non-local and gradient effects are essential for very high natural frequencies [12,19] and low aspect ratios and diameters [20,25], then these size effects are neglected in the present paper, which is focused on low-frequency vibrations of SWNTs with large aspect ratios and diameters. About the presence of surface effects, it was found that they arise only in the nanocomposites; conversely, they are not present in the isolated CNTs [13], studied in this paper, which, on the other hand, can be applied in a very large number of nanoscale devices.

3. Sanders-Koiter shell theory (numerical solution)

First of all, it must be pointed out that in the present theory the size-effects are not considered; this simplification gives some limitations to the present model in terms of type of nanotube and dynamic conditions. The small scale effect has a significant influence on the dispersion of the flexural waves of SWNTs only for high frequencies [12]. Besides, the effect of nonlocal parameter on the natural frequency is significant only for the SWNTs with low aspect ratio and small diameter [20]. Therefore, in order to make valid the assumptions of the present theory, the following two limitations have to be considered: the low part of the frequency spectrum can be analysed [19], carbon nanotubes with high aspect ratio and large diameter can be studied [25].

In Figure 1, a circular cylindrical shell having radius R, length L and thickness h is represented; a cylindrical coordinate system (O; x, θ, z) is considered in order to take advantage from the axial symmetry of the structure, the origin O of the reference system is located at the centre of one end of the cylindrical shell. In Figure 1, three displacement fields are represented: longitudinal u (x, θ, t), circumferential v (x, θ, t) and radial w (x, θ, t); the radial displacement field w is considered positive outward and (x, θ) are the longitudinal and angular coordinates of an arbitrary point on the middle surface of the shell; z is the radial coordinate along the thickness h; t is the time.

3.1. Strain-displacement relationships

It should be pointed out that, due to the nanoscale, CNTs present huge natural frequencies (THz) and infinitesimal dimensions; this can induce numerical troubles to numerical algorithms if the governing equations are not transformed into a nondimensional form.

Here, the three displacement fields (u, v, w) are nondimensionalized by means of the radius R of the carbon nanotube

$$u = R\tilde{u} \qquad v = R\tilde{v} \qquad w = R\tilde{w} \tag{3}$$

where ($\tilde{u}$, $\tilde{v}$, $\tilde{w}$) are the nondimensional displacement fields.

In the Sanders-Koiter elastic thin shell theory, the transverse shear strains (γ_{xz}, $\gamma_{\theta z}$) are neglected (Kirchhoff-Love's kinematic hypothesis). The tangential normal strains (ε_x, ε_θ) and the tangential shear strain $\gamma_{x\theta}$ at an arbitrary radius on the shell thickness are related to the middle surface strains ($\varepsilon_{x,0}$, $\varepsilon_{\theta,0}$, $\gamma_{x\theta,0}$) and to the changes in curvature and torsion of the middle surface of the shell (k_x, k_θ, $k_{x\theta}$) by the relationships [38]

$$\varepsilon_x = \varepsilon_{x,0} + zk_x \qquad \varepsilon_\theta = \varepsilon_{\theta,0} + zk_\theta \qquad \gamma_{x\theta} = \gamma_{x\theta,0} + zk_{x\theta} \tag{4}$$

where z is the distance of the arbitrary point on the thickness from the middle surface of the shell, according to the condition ($-h/2 \le z \le h/2$), as shown in Figure 1.

The middle surface strains ($\varepsilon_{x,0}$, $\varepsilon_{\theta,0}$, $\gamma_{x\theta,0}$) are nondimensional parameters. The changes in curvature and torsion of the middle surface of the shell (k_x, k_θ, $k_{x\theta}$) are dimensional parameters, and they must be written in nondimensional form; this is achieved by considering the radius R. The middle surface strains and nondimensional changes in curvature and torsion can be written as follows [38]

$$\tilde{\varepsilon}_{x,0} = \alpha \frac{\partial \tilde{u}}{\partial \eta} = \varepsilon_{x,0} \qquad \tilde{\varepsilon}_{\theta,0} = \frac{\partial \tilde{v}}{\partial \theta} + \tilde{w} = \varepsilon_{\theta,0} \qquad \tilde{\gamma}_{x\theta,0} = \frac{\partial \tilde{u}}{\partial \theta} + \alpha \frac{\partial \tilde{v}}{\partial \eta} = \gamma_{x\theta,0} \tag{5}$$

$$\tilde{k}_x = -\alpha^2 \frac{\partial^2 \tilde{w}}{\partial \eta^2} = Rk_x \qquad \tilde{k}_\theta = \frac{\partial \tilde{v}}{\partial \theta} - \frac{\partial^2 \tilde{w}}{\partial \theta^2} = Rk_\theta \qquad \tilde{k}_{x\theta} = -2\alpha \frac{\partial^2 \tilde{w}}{\partial \eta \partial \theta} + \frac{3}{2}\alpha \frac{\partial \tilde{v}}{\partial \eta} - \frac{1}{2}\frac{\partial \tilde{u}}{\partial \theta} = Rk_{x\theta} \tag{6}$$

where $(\tilde{\varepsilon}_{x,0}, \tilde{\varepsilon}_{\theta,0}, \tilde{\gamma}_{x\theta,0}) = (\varepsilon_{x,0}, \varepsilon_{\theta,0}, \gamma_{x\theta,0})$ are middle surface strains of the shell, $(\tilde{k}_x, \tilde{k}_\theta, \tilde{k}_{x\theta})$ are the nondimensional middle surface changes in curvature and torsion, $\eta = x / L$ is the nondimensional longitudinal coordinate of the shell and $\alpha = R / L$.

3.2. Force and moment resultants

The nondimensional force ($\tilde{N}_x, \tilde{N}_\theta, \tilde{N}_{x\theta}, \tilde{Q}_x, \tilde{Q}_\theta$) and moment ($\tilde{M}_x, \tilde{M}_\theta, \tilde{M}_{x\theta}$) resultants can be written in the following form [39]

$$\tilde{N}_x = \tilde{\varepsilon}_{x,0} + \nu \tilde{\varepsilon}_{\theta,0} = \frac{N_x}{J} \qquad \tilde{N}_\theta = \tilde{\varepsilon}_{\theta,0} + \nu \tilde{\varepsilon}_{x,0} = \frac{N_\theta}{J} \qquad \tilde{N}_{x\theta} = \frac{(1-\nu)}{2}\tilde{\gamma}_{x\theta,0} = \frac{N_{x\theta}}{J} \tag{7}$$

$$\tilde{Q}_x = R\left[\tilde{k}_{x,x} + \nu \tilde{k}_{\theta,x} + \frac{(1-\nu)}{2R}\tilde{k}_{\theta x,\theta}\right] = \frac{R^2}{D}Q_x \qquad \tilde{Q}_\theta = R\left[\frac{(1-\nu)}{2}\tilde{k}_{x\theta,x} + \frac{1}{R}\left(\tilde{k}_{\theta,\theta} + \nu \tilde{k}_{x,\theta}\right)\right] = \frac{R^2}{D}Q_\theta \tag{8}$$

$$\tilde{M}_x = \tilde{k}_x + \nu \tilde{k}_\theta = \frac{R}{D}M_x \qquad \tilde{M}_\theta = \tilde{k}_\theta + \nu \tilde{k}_x = \frac{R}{D}M_\theta \qquad \tilde{M}_{x\theta} = \frac{(1-\nu)}{2}\tilde{k}_{x\theta} = \frac{R}{D}M_{x\theta} \tag{9}$$

where ($N_x, N_\theta, N_{x\theta}, Q_x, Q_\theta$) are the force resultants per unit length of the shell, ($M_x, M_\theta, M_{x\theta}$) are the moment resultants per unit length of the shell, $J = Eh/(1-\nu^2)$ and $D = Eh^3/(12(1-\nu^2))$.

3.3. Elastic strain energy

According to the Sanders-Koiter theory, the elastic strain energy U of a circular cylindrical shell is written in the form [41]

$$U = \frac{1}{2} LR \int_0^1 \int_0^{2\pi} \int_{-h/2}^{h/2} (\sigma_x \varepsilon_x + \sigma_\theta \varepsilon_\theta + \tau_{x\theta} \gamma_{x\theta})\, d\eta d\theta dz \tag{10}$$

The elastic strain energy U can be nondimensionalized, let $\tilde{U}$ be the nondimensional elastic strain energy, it can be expressed in the form

$$\begin{aligned} \tilde{U} = \frac{1}{2} \frac{1}{1-\nu^2} \Bigg[& \int_0^1 \int_0^{2\pi} \left(\tilde{\varepsilon}_{x,0}^2 + \tilde{\varepsilon}_{\theta,0}^2 + 2\nu \tilde{\varepsilon}_{x,0} \tilde{\varepsilon}_{\theta,0} + \frac{(1-\nu)}{2} \tilde{\gamma}_{x\theta,0}^2 \right) d\eta d\theta \\ & + \frac{\beta^2}{12} \int_0^1 \int_0^{2\pi} \left(\tilde{k}_x^2 + \tilde{k}_\theta^2 + 2\nu \tilde{k}_x \tilde{k}_\theta + \frac{(1-\nu)}{2} \tilde{k}_{x\theta}^2 \right) d\eta d\theta \Bigg] = \frac{U}{A} \end{aligned} \tag{11}$$

where $A = EhLR$ and $\beta = h / R$.

3.4. Kinetic energy

The kinetic energy T of a cylindrical shell (rotary inertia effect being neglected) is given by [41]

$$T = \frac{1}{2} \rho hLR \int_0^1 \int_0^{2\pi} (\dot{u}^2 + \dot{v}^2 + \dot{w}^2)\, d\eta d\theta \tag{12}$$

where ρ is the mass density of the shell and the overdot denotes a time derivative.

The time variable t can be nondimensionalized by introducing a reference natural frequency ω_0 in the following form [38]

$$t = \omega_0^{-1} \tau \qquad\qquad \omega_0 = \sqrt{\frac{E}{(1-\nu^2)\rho R^2}} \tag{13}$$

where τ is the nondimensional time variable.

The velocity fields $(\dot{u}, \dot{v}, \dot{w})$ can be nondimensionalized by considering the radius R and the reference natural frequency ω_0 in the following form

$$\dot{u} = R\omega_0 \tilde{u}' \qquad\qquad \tilde{u}' = \frac{d\tilde{u}}{d\tau} \tag{14}$$

$$\dot{v} = R\omega_0 \tilde{v}' \qquad\qquad \tilde{v}' = \frac{d\tilde{v}}{d\tau} \tag{15}$$

$$\dot{w} = R\omega_0 \tilde{w}' \qquad \tilde{w}' = \frac{d\tilde{w}}{d\tau} \tag{16}$$

where ($\tilde{u}'$, $\tilde{v}'$, $\tilde{w}'$) are the nondimensional velocity fields.

Let $\tilde{T}$ be the nondimensional kinetic energy, which is expressed in the form

$$\tilde{T} = \frac{1}{2}\int_0^1\int_0^{2\pi}(\tilde{u}'^2 + \tilde{v}'^2 + \tilde{w}'^2)d\eta d\theta = \frac{1}{2}\int_0^1\int_0^{2\pi}\left[\left(\frac{d\tilde{u}}{d\tau}\right)^2 + \left(\frac{d\tilde{v}}{d\tau}\right)^2 + \left(\frac{d\tilde{w}}{d\tau}\right)^2\right]d\eta d\theta = \frac{T}{\gamma A} \tag{17}$$

where $\gamma = \rho R^2 {\omega_0}^2 / E$.

3.5. Linear vibration analysis (complete Sanders-Koiter shell theory)

In the linear vibration analysis, the three nondimensional displacement fields are expanded by using a double mixed series, then the Rayleigh-Ritz method is applied to the linearized formulation of the problem, in order to obtain approximated eigenfunctions. The linear vibration analysis is carried out considering only the quadratic terms in equation (10).

A modal vibration, i.e., a synchronous motion, can be formally written in the form [43]

$$\tilde{u}(\eta,\theta,\tau) = \tilde{U}(\eta,\theta)\,f(\tau) \qquad \tilde{v}(\eta,\theta,\tau) = \tilde{V}(\eta,\theta)\,f(\tau) \qquad \tilde{w}(\eta,\theta,\tau) = \tilde{W}(\eta,\theta)\,f(\tau) \tag{18}$$

where $\tilde{U}(\eta, \theta)$, $\tilde{V}(\eta, \theta)$, $\tilde{W}(\eta, \theta)$ describe the mode shape of the shell and $f(\tau)$ represents the common time law, which is supposed to be the same for each displacement field in the modal vibration analysis.

The mode shape ($\tilde{U}$, $\tilde{V}$, $\tilde{W}$) is expanded by means of a double mixed series, in terms of m-th order Chebyshev polynomials $T_m^*(\eta)$ in the axial direction and harmonic functions (cos $n\theta$, sin $n\theta$) in the circumferential direction, in the following form [43]

$$\tilde{U}(\eta,\theta) = \sum_{m=0}^{M_u}\sum_{n=0}^{N}\tilde{U}_{m,n}T_m^*(\eta)\cos n\theta \tag{19}$$

$$\tilde{V}(\eta,\theta) = \sum_{m=0}^{M_v}\sum_{n=0}^{N}\tilde{V}_{m,n}T_m^*(\eta)\sin n\theta \tag{20}$$

$$\tilde{W}(\eta,\theta) = \sum_{m=0}^{M_w}\sum_{n=0}^{N}\tilde{W}_{m,n}T_m^*(\eta)\cos n\theta \tag{21}$$

where $T_m^* = T_m(2\eta - 1)$, m is the polynomials degree, n denotes the number of nodal diameters and ($\tilde{U}_{m,n}$, $\tilde{V}_{m,n}$, $\tilde{W}_{m,n}$) are unknown coefficients.

3.5.1. Boundary conditions

Clamped and free SWNTs are now analysed; the boundary conditions are imposed by applying constraints to the unknown coefficients ($\tilde{U}_{m,n}$, $\tilde{V}_{m,n}$, $\tilde{W}_{m,n}$) of the expansions (19), (20), (21).

3.5.1.1. Clamped-clamped

Clamped – clamped boundary conditions are given by [43]

$$\tilde{u} = 0 \qquad \tilde{v} = 0 \qquad \tilde{w} = 0 \qquad \tilde{w}_{,\eta} = 0 \qquad \eta = 0,1 \tag{22}$$

where $(\cdot)_{,\eta} = \partial(\cdot)/\partial\eta$.

The previous conditions imply the following equations [43]

$$\sum_{m=0}^{M_u} \tilde{U}_{m,n} T_m^*(\eta) = 0 \qquad \theta \in [0, 2\pi] \qquad n \in [0, N] \tag{23}$$

$$\sum_{m=0}^{M_v} \tilde{V}_{m,n} T_m^*(\eta) = 0 \qquad \theta \in [0, 2\pi] \qquad n \in [0, N] \tag{24}$$

$$\sum_{m=0}^{M_w} \tilde{W}_{m,n} T_m^*(\eta) = 0 \qquad \theta \in [0, 2\pi] \qquad n \in [0, N] \tag{25}$$

$$\sum_{m=0}^{M_w} \tilde{W}_{m,n} T_{m,\eta}^*(\eta) = 0 \qquad \theta \in [0, 2\pi] \qquad n \in [0, N] \tag{26}$$

The linear algebraic system given by the equations (23-26) can be solved analytically in terms of the coefficients ($\tilde{U}_{0,n}$, $\tilde{U}_{1,n}$, $\tilde{V}_{0,n}$, $\tilde{V}_{1,n}$, $\tilde{W}_{0,n}$, $\tilde{W}_{1,n}$, $\tilde{W}_{2,n}$, $\tilde{W}_{3,n}$), for n $\in$ [0, N].

3.5.1.2. Free-free

Free – free boundary conditions are given by [43]

$$\tilde{N}_x = 0 \qquad \tilde{N}_{x\theta} + \tilde{M}_{x\theta} = 0 \qquad \tilde{Q}_x + \frac{\partial \tilde{M}_{x\theta}}{\partial \theta} = 0 \qquad \tilde{M}_x = 0 \qquad \eta = 0,1 \tag{27}$$

It can be observed that the boundary conditions (27) applied at the free edges of the SWNTs are of natural type; since the Rayleigh-Ritz method is used for finding the solution, just the geometric boundary conditions have to be exactly satisfied: it means that it is not necessary to satisfy the

natural conditions (27) by the expansions (19), (20), (21) since they will be satisfied by the minimization of the energy of the system.

3.5.2. Rayleigh-Ritz method

The maximum number of variables needed for describing a general vibration mode with n nodal diameters is obtained by the relation ($N_p = M_u + M_v + M_w + 3 - p$), where ($M_u = M_v = M_w$) denote the degree of the Chebyshev polynomials and p describes the number of equations needed to satisfy the boundary conditions.

A specific convergence analysis is carried out to select the degree of the Chebyshev polynomials: degree 11 is found suitably accurate, ($M_u = M_v = M_w = 11$), see Refs. [41-43] for the details.

For a multi-mode analysis including different values of nodal diameters n, the number of degrees of freedom of the system is computed by the relation ($N_{max} = N_p \times (N + 1)$), where N represents the maximum value of the nodal diameters n considered.

For example, in the case of a SWNT with free edges ($p = 0$), the number of degrees of freedom of the system with ($n = 2$) nodal diameters is equal to ($N_{max} = N_p \times (N + 1) = 36 \times (2 + 1) = 108$).

Equations (18) are inserted into the expressions of the elastic strain energy $\tilde{U}$, eq. (11), and kinetic energy $\tilde{T}$, eq. (17), to compute the Rayleigh quotient $R(\tilde{\mathrm{q}}) = \tilde{U}_{\max} / \tilde{T}^*$, where $\tilde{U}_{\max} = \max(\tilde{U})$ is the maximum of the potential energy during a modal vibration, $\tilde{T}^* = \tilde{T}_{\max} / \omega^2$, $\tilde{T}_{\max} = \max(\tilde{T})$ is the maximum of the kinetic energy during a modal vibration, ω represents the circular frequency of the synchronous harmonic motion $f(\tau) = \cos \omega\tau$; $\tilde{\mathrm{q}}$ is a vector containing all the unknown variables (its structure depends on the boundary conditions) [43]

$$\tilde{\mathrm{q}} = \begin{bmatrix} \dots \\ \tilde{U}_{m,m} \\ \tilde{V}_{m,n} \\ \tilde{W}_{m,n} \\ \dots \end{bmatrix} \tag{28}$$

After imposing the stationarity to the Rayleigh quotient, one obtains the eigenvalue problem [43]

$$(-\omega^2 \tilde{\mathrm{M}} + \tilde{\mathrm{K}})\tilde{\mathrm{q}} = \tilde{0} \tag{29}$$

which furnishes approximate natural frequencies (eigenvalues) and mode shapes (eigenvectors and eigenfunctions).

The approximate mode shape of the *j*-th mode is given by the equations (19), (20), (21), where the coefficients ($\tilde{U}_{m,n}$, $\tilde{V}_{m.n}$, $\tilde{W}_{m,n}$) are substituted with ($\tilde{U}^{(j)}_{m,n}$, $\tilde{V}^{(j)}_{m,n}$, $\tilde{W}^{(j)}_{m,n}$), which denote the components of the *j*-th eigenvector $\tilde{\mathrm{q}}_j$ of the equation (29).

The vector function [43]

$$\tilde{\mathrm{Q}}^{(j)}(\eta,\theta)=\begin{bmatrix}\tilde{U}^{(j)}(\eta,\theta)\\ \tilde{V}^{(j)}(\eta,\theta)\\ \tilde{W}^{(j)}(\eta,\theta)\end{bmatrix} \tag{30}$$

is the approximation of the *j*-th eigenfunction vector of the original problem.

4. Reduced Sanders-Koiter shell theory (analytical solution)

In the present section, a reduced form of the Sanders-Koiter shell theory is developed. Also in this model, the transverse shear strains (γ_{xz}, $\gamma_{\theta z}$) are neglected. In the present work, we consider small amplitude vibrations of CNTs, and a potential energy is predominantly due to bending, torsion and longitudinal tensions. Therefore, we can suppose that both in-plane circumferential normal strain and tangential shear strain of the middle surface of the shell ($\varepsilon_{\theta,0}$, $\gamma_{x\theta,0}$) are "small differences of relatively large quantities" [38], and they can be neglected. Due to this assumption, one can reduce the number of dependent variables; both the longitudinal and the circumferential displacements can be expressed via the radial one.

By assuming the linear expansions of the longitudinal $\tilde{u}$, circumferential $\tilde{v}$ and radial $\tilde{w}$ displacement fields as

$$\tilde{u}(\eta,\theta,\tau) = \hat{U}(\eta)\cos(n\theta)\mathrm{e}^{-\mathrm{i}\omega\tau} \tag{31}$$

$$\tilde{v}(\eta,\theta,\tau) = \hat{V}(\eta)\sin(n\theta)\mathrm{e}^{-\mathrm{i}\omega\tau} \tag{32}$$

$$\tilde{w}(\eta,\theta,\tau) = \hat{W}(\eta)\cos(n\theta)\mathrm{e}^{-\mathrm{i}\omega\tau} \tag{33}$$

using the condition of absence of ring (in-plane circumferential) deformation effects

$$\tilde{\varepsilon}_{\theta,0} = \frac{\partial\tilde{v}}{\partial\theta} + \tilde{w} = 0 \tag{34}$$

and the condition of absence of tangential shear deformation effects

$$\tilde{\gamma}_{x\theta,0} = \frac{\partial\tilde{u}}{\partial\theta} - \alpha\frac{\partial\tilde{v}}{\partial\eta} = 0 \tag{35}$$

we can obtain the following expressions for the nondimensional variables $\hat{V}$ and $\hat{U}$ as functions of the radial displacement $\hat{W}$

$$\hat{V}(\eta) = -\frac{\hat{W}(\eta)}{n} \tag{36}$$

$$\hat{U}(\eta) = -\frac{\alpha}{n^2}\frac{\partial\hat{W}(\eta)}{\partial\eta} \tag{37}$$

4.1. Equations of motion

In order to get the adequate equation of motion in terms of $\hat{W}$ one cannot insert these relations into equations of motion (1.120) of Ref. [38] because of the "reactive" nature of the circumferential and tangential shear reduced forces. Therefore, we have to start from the following "force" form of the equations of motion

$$\frac{\partial^2 \tilde{u}}{\partial \tau^2} - \alpha \frac{\partial \tilde{N}_x}{\partial \eta} - \frac{\partial \tilde{N}_{x\theta}}{\partial \theta} + \frac{\beta}{2} \frac{\partial \tilde{M}_{x\theta}}{\partial \theta} = 0 \tag{38}$$

$$\frac{\partial^2 \tilde{v}}{\partial \tau^2} - \frac{\partial \tilde{N}_\theta}{\partial \theta} - \alpha \frac{\partial \tilde{N}_{x\theta}}{\partial \eta} - \beta \frac{\partial^2 \tilde{M}_\theta}{\partial \theta^2} - \frac{3}{2} \alpha\beta \frac{\partial \tilde{M}_{x\theta}}{\partial \eta} = 0 \tag{39}$$

$$\frac{\partial^2 \tilde{w}}{\partial \tau^2} + \tilde{N}_\theta - \alpha^2 \beta \frac{\partial^2 \tilde{M}_x}{\partial \eta^2} - \beta \frac{\partial^2 \tilde{M}_\theta}{\partial \theta^2} - 2\alpha\beta \frac{\partial^2 \tilde{M}_{x\theta}}{\partial \eta \partial \theta} = 0 \tag{40}$$

where $(\tilde{N}_x, \tilde{N}_\theta, \tilde{N}_{x\theta})$ and $(\tilde{M}_x, \tilde{M}_\theta, \tilde{M}_{x\theta})$ are the reduced force and moment resultants, respectively.

The procedure of the equations reduction consists of a consecutive definition of the expressions for $\tilde{N}_{x\theta}$ and $\tilde{N}_\theta$ from the equations (38) and (39), and their substitution into the equation (40).

Let us consider these actions in detail.

We take into account that the reduced forces and momenta have the following form

$$\tilde{N}_x(\eta, \theta, \tau) = \varphi_\eta(\eta) \cos(n\theta) \mathrm{e}^{-\mathrm{i}\omega\tau} \tag{41}$$

$$\tilde{N}_\theta(\eta, \theta, \tau) = \varphi_\theta(\eta) \cos(n\theta) \mathrm{e}^{-\mathrm{i}\omega\tau} \tag{42}$$

$$\tilde{N}_{x\theta}(\eta, \theta, \tau) = \varphi_{\eta\theta}(\eta) \sin(n\theta) \mathrm{e}^{-\mathrm{i}\omega\tau} \tag{43}$$

$$\tilde{M}_x(\eta, \theta, \tau) = \mu_\eta(\eta) \cos(n\theta) \mathrm{e}^{-\mathrm{i}\omega\tau} \tag{44}$$

$$\tilde{M}_\theta(\eta, \theta, \tau) = \mu_\theta(\eta) \cos(n\theta) \mathrm{e}^{-\mathrm{i}\omega\tau} \tag{45}$$

$$\tilde{M}_{x\theta}(\eta, \theta, \tau) = \mu_{\eta\theta}(\eta) \sin(n\theta) \mathrm{e}^{-\mathrm{i}\omega\tau} \tag{46}$$

Substituting these relationships into equations (38-40), we obtain the relations

$$-\omega^2 \hat{U} - \alpha \frac{\partial \varphi_\eta}{\partial \eta} - n\varphi_{\eta\theta} + n \frac{\beta}{2} \mu_{\eta\theta} = 0 \tag{47}$$

$$-\omega^2\hat{V} + n\varphi_\theta - \alpha n\frac{\partial\varphi_{\eta\theta}}{\partial\eta} + \beta n^2\mu_\theta - \frac{3}{2}\alpha\beta\frac{\partial\mu_{\eta\theta}}{\partial\eta} = 0 \tag{48}$$

$$-\omega^2\hat{W} + \varphi_\theta - \alpha^2\beta\frac{\partial^2\mu_\eta}{\partial\eta^2} + \beta n^2\mu_\theta - 2\alpha\beta n\frac{\partial\mu_{\eta\theta}}{\partial\eta} = 0 \tag{49}$$

Then, we can obtain $\varphi_{\eta\theta}$ from equation (47) and substitute the result into equation (48), the same procedure applies to φ_θ that is substituted into equation (49).

The last step is to express the remaining reduced forces and momenta via the corresponding deformations excluding the variables $\hat{V}$ and $\hat{U}$ by the relations (36) and (37), respectively.

The final equation of motion for the nondimensional radial displacement field $\hat{W}$ is given by

$$\begin{aligned}&\frac{\partial^2\hat{W}}{\partial\tau^2} + \frac{n^2(n^2-1)^2}{n^2+1}\beta^2\hat{W} - \frac{(n^2-1)(n^2-1+\nu)}{6(n^2+1)}\alpha^2\beta^2\frac{\partial^2\hat{W}}{\partial\eta^2}\\ &-\frac{\alpha^2}{n^2(n^2+1)}\frac{\partial^4\hat{W}}{\partial\tau^2\partial\eta^2} + \frac{12+n^4\beta^2}{12n^2(n^2+1)}\alpha^4\frac{\partial^4\hat{W}}{\partial\eta^4} = 0\end{aligned} \tag{50}$$

where the time dependence of the radial displacement is taken into account explicitly.

The same equation can be obtained taking into account only the bending, torsion and longitudinal stresses in the expression of the strain energy and expressing the longitudinal and circumferential displacements via the radial one before the application of the variational procedure.

4.2. Boundary conditions

In the present section, both periodic and free-free boundary conditions are considered.

4.2.1. Periodic boundary conditions

In the case of periodic boundary conditions, equation (50) leads to the dispersion equation

$$\omega^2 = \frac{\beta^2n^4(n^2-1)^2 + 2\alpha^2\beta^2\pi^2j^2n^2(n^2-1)(n^2-(1-\nu)) + \alpha^4(12+\beta^2n^4)\pi^4j^4}{12(n^4+n^2+\alpha^2\pi^2j^2)} \tag{51}$$

where j describes the number of half-waves along the CNT axis.

4.2.2. Free-free boundary conditions

Using equation (50) and assuming $\hat{W} = \bar{W} e^{i\omega\tau}$ one obtains

$$-\omega^2 \bar{W} + \Omega^2 \bar{W} - c^2 \frac{\partial^2 \bar{W}}{\partial \eta^2} + \omega^2 A \frac{\partial^2 \bar{W}}{\partial \eta^2} + B \frac{\partial^4 \bar{W}}{\partial \eta^4} = 0 \tag{52}$$

where

$$\Omega^2 = \frac{n^2 (n^2 - 1)^2}{12(n^2 + 1)} \beta^2 \qquad c^2 = \frac{(n^2 - 1)(n^2 - 1 + \nu)}{6(n^2 + 1)} \alpha^2 \beta^2 \tag{53}$$

$$A = \frac{\alpha^2}{n^2 (n^2 + 1)} \qquad B = \frac{12 + n^4 \beta^2}{12 n^2 (n^2 + 1)} \alpha^4 \tag{54}$$

We can factorize equation (52) as follows

$$B \left(\frac{\partial^2}{\partial \eta^2} + \mu^2 \right) \left(\frac{\partial^2}{\partial \eta^2} - \gamma^2 \right) \bar{W} = 0 \tag{55}$$

where the parameters μ and γ are coupled by the relations

$$\mu^2 \gamma^2 = \frac{\omega^2 - \Omega^2}{B} \qquad \mu^2 - \gamma^2 = \frac{\omega^2 A - c^2}{B} \tag{56}$$

The general solution of equation (55) contains both a harmonic-type solution and an aperiodic exponential-type one in η; the latter one plays the role of the edge layer, where the parameter γ specifies its magnitude. In such a case the parameter μ is an effective wave number.

This equation should be completed with the free-free boundary conditions at (η = 0) and (η = 1), in terms of the radial displacement $\bar{W}$.

The first boundary condition corresponds to the absence of bending moment $\tilde{M}_x$ at the free edges of the carbon nanotube, which leads to the following relation

$$\tilde{M}_x = 0 \;\Rightarrow\; \alpha^2 \frac{\partial^2 \bar{W}}{d\eta^2} - \nu (n^2 - 1) \bar{W} = 0 \qquad \eta = (0,1) \tag{57}$$

The second boundary condition is related with the transverse force $\tilde{Q}_x$ combined with the torsional moment $\tilde{M}_{x\theta}$ at the free edges of the carbon nanotube, and it leads to the following relation

$$\tilde{Q}_x + \frac{1}{R}\frac{\partial \tilde{M}_{x\theta}}{\partial \theta} = 0 \;\Rightarrow\; \alpha^2 \frac{\partial^3 \bar{W}}{\partial \eta^3} - (n^2 - 1)(2 - \nu)\frac{\partial \bar{W}}{\partial \eta} = 0 \qquad \eta = (0,1) \tag{58}$$

It should be noted that the two remaining boundary conditions are

$$\tilde{N}_x = 0 \qquad \tilde{N}_{x\theta} + \tilde{M}_{x\theta} = 0 \tag{59}$$

such conditions are satisfied thanks to the exclusion procedure discussed above.

4.3. General solution

The general solution of the equation (55) can be written as follows

$$\bar{W}(\eta) = c_1 \cos(\mu\eta + \delta_1) + c_2 \exp(-\gamma\eta + \delta_2) + c_3 \exp(\gamma\eta + \delta_3) \tag{60}$$

where (c_1, c_2, c_3) and (δ_1, δ_2, δ_3) are nondimensional parameters to be determined.

In equation (60), there are both symmetric and asymmetric constituents corresponding to an even and odd number of half-waves along the η-axis of the CNT.

The respective values of the nondimensional parameters for the symmetric solution (even number of longitudinal half-waves) are

$$c_2 = c_3 \qquad \delta_1 = -\frac{\mu}{2} \qquad \delta_2 = \delta_3 = -\frac{\gamma}{2} \tag{61}$$

and in the asymmetric one (odd number of longitudinal half-waves) we have

$$c_2 = -c_3 \qquad \delta_1 = -\frac{\mu}{2} - \frac{\pi}{2} \qquad \delta_2 = \delta_3 = -\frac{\gamma}{2} \tag{62}$$

We can rewrite the symmetric and asymmetric solutions as follows

$$\bar{W}_s = \cos[\mu(\eta - 1/2)] + b\sinh^2\left[\frac{\gamma}{2}(\eta - 1/2)\right] \tag{63}$$

$$\bar{W}_a = \sin[\mu(\eta - 1/2)] + b\sinh\left[\gamma(\eta - 1/2)\right] \tag{64}$$

where the parameter *b* plays the role of the edge layer amplitude.

By substituting these expressions into relations (57) and (58), we finally obtain two transcendent equations with respect to parameters μ and *b*, which must be solved numerically.

5. Numerical results

In Table 1, effective and equivalent parameters of Single-Walled Carbon Nanotubes are reported [28]. These parameters are used to carry out comparisons with experiments and MD simulations, i.e. the model validation.

The diameter D of a CNT can be directly calculated from its chirality indices (r, s) as follows

$$D = \frac{a}{\pi}\sqrt{(r^2 + rs + s^2)} \tag{65}$$

r and s identify the chiral vector, which gives the rolling direction of a honeycomb crystal lattice of graphene; a = 0.246 nm.

Therefore, a carbon nanotube modelled as a thin circular cylindrical shell is uniquely described by the length L and by the indices (r, s), which allow to determine the CNT diameter D. L and D are mutually connected by the aspect ratio $\chi = L / D$. Therefore, (r, s, χ) are the independent variables of a SWNT.

5.1. Validation of the numerical approach in linear field

In this section, the numerical model based on the Sanders-Koiter shell theory is validated in linear field. The natural frequencies of the carbon nanotubes based on this theory are compared with data available in the literature: experiments, Molecular Dynamics (MD) simulations and Finite Element Analyses (FEA). In Tables 2-5 all the comparisons are reported. These comparisons show that the Sanders-Koiter theory and the present approach of solution give excellent results in terms of natural frequencies. Furthermore, this proves that the equivalent parameters are correct. In the following subsections, detailed comments regarding this validation are given.

5.1.1. Radial Breathing Mode (RBM)

The RBM is the specific vibrational mode which is often used in order to identify experimentally the CNTs by Resonant Raman Spectroscopy.

This mode corresponds to the “vibrational” numbers (j = 0, n = 0), and its natural frequency can be easily calculated in the framework of the Sanders-Koiter elastic shell theory. The RBM appears only in the case of free-free boundary conditions.

The existing data for vibrations of CNTs are mainly focused on the radial breathing mode of SWNTs and MWNTs because the spectrum of nanotubes is quite complex. Moreover, the natural

frequency associated with the radial breathing mode of SWNTs is inversely proportional to the tube diameter and independent from the length (aspect ratio χ) and chirality (symmetry) of the nanotube.

For the radial breathing mode, the radial displacement field $\tilde{w}(\eta, \theta, \tau)$ is spatially uniform, i.e., it is independent of η and θ ($\tilde{w} = \tilde{w}(\tau)$). In this special case, the bending stiffness of the SWNTs does not appear because the radial breathing vibration does not involve the bending deformation and corresponds to an uniaxial stress state of the graphene sheet.

Resonant Raman Spectroscopy (RRS) provides a powerful technique to study the quantum properties of electrons and phonons in carbon nanotubes and to determine their atomic structure, i.e., the chirality indices (*r*, *s*), of an isolated SWNT. The radial breathing mode exhibits strong resonant characteristics in the Raman spectra, because it corresponds to the symmetric in-phase motion of all the carbon atoms in the radial direction of the tube. In this configuration all the carbon atoms undergo the same radial displacement.

The RRS of a SWNT allows a unique assignment of its chirality to be made by measuring the RBM frequency ω_{RBM} and using the theory of the resonant transitions. By considering the frequency and the intensity of the RBM mode in the RRS spectra, it is possible to assign the correct chirality (*r*, *s*) to the resonant SWNT.

The natural frequencies of the radial breathing vibration mode based on the present numerical model are in good agreement with the experimental RRS results. Table 2 presents a comparison for different armchair, zigzag and chiral SWNTs under free-free boundary conditions, relative errors are less than 5%, it appears a satisfactory accuracy.

Molecular Dynamics Simulations (MDS) allow to study the free vibrations of armchair, zigzag and chiral SWNTs with different geometries and boundary conditions, taking into account the atomic structure and the potential energy of the carbon atoms.

Three stiffness parameters, i.e., the tensile resistance *EA*, the flexural rigidity *EI* and the torsional stiffness *GJ* need to be determined for the deformation analysis in the MDS, where *E* and *G* are the Young's and shear moduli, *A* and *J* are the cross-section area and polar inertia of the equivalent beam.

The interaction between carbon atoms is specified by using the MD potentials associated with bond stretching, changes in angles between adjacent bonds, bond torsion and inversion, Van der Waals and electrostatic interactions, coupling among stretching, bending and torsional deformations.

Results based on the present numerical model for different armchair and zigzag SWNTs under free-free boundary conditions are shown in Table 3. The present numerical model is in good agreement with the MDS of radial breathing modes, with relative errors less than 4%.

5.1.2. Beam-Like Modes (BLMs)

The accuracy of the present numerical model is now assessed for beam-like modes (n = 1) by means of comparisons with MD simulations and FE analyses.

The natural frequencies of the beam-like modes obtained with the present numerical model are in good agreement with the MDS results. The comparisons shown in Table 4 for an armchair (5, 5) SWNT with different aspect ratios χ under clamped-free and clamped-clamped boundary conditions denote relative errors smaller than 5%.

In particular, in Table 4 it may be seen that the percent difference between the present theory and MDS, for the first four flexural modes, decreases as the length of the nanotube increases, i.e., when the influence of the boundary conditions on the natural frequencies is reduced. Furthermore, the natural frequencies under clamped-free boundary conditions are greater than those under clamped-clamped boundary conditions for the correspondent vibration modes.

The atomistic Finite Element (FE) model of the SWNTs is based on the equivalent structural beam elements and concentrated masses. Time efficiency and computational simplicity are the advantages of FE method in comparison with other atomistic simulation approaches, such as classical MDS, in the study of natural frequencies and mode shapes of the SWNTs.

In FE analyses, the beam elements represent the joints of the covalent bonds, where the beam length is assumed to be equal to the covalent bond distance of the carbon atoms in the hexagonal lattice. The elastic properties (extensional, bending and torsional stiffness) of the beam element are calculated to simulate the interatomic covalent forces and the potential energies of the CNT.

On the other hand, the concept of concentrated masses is adopted to simulate the carbon atoms. They are located at the ends of the beam elements connecting the carbon atoms, forming hexagonal cells on the nanotube surface: natural frequencies and mode shapes are then obtained through the eigen-analysis of the lattice cylindrical shell structure by considering mass and stiffness matrices.

Results based on the present shell theory are compared with FEA results found in literature, Table 5. Different zigzag SWNTs with various aspect ratios χ under clamped-free and clamped-clamped boundary conditions are investigated. The present numerical model is in good agreement with the atomistic FEA for beam-like vibration modes, with relative errors less than 6%. Also in the present case, the percent difference between the present method and FEA analyses, for the first four flexural modes, decreases as the length of the nanotube increases, when the influence of the boundary conditions on the natural frequencies is reduced. Again, the natural frequencies under clamped-free boundary conditions are greater than those under clamped-clamped boundary conditions.

5.2. Dispersion curves of the analytical approach

In this section, the accuracy of the analytical model based on the reduced Sanders-Koiter theory is studied. The equivalent parameters of Table 1 are used and numerical solutions of the transcendent equations for zigzag (10, 0) SWNTs of various lengths are obtained.

In Figure 2 the eigenfrequencies, calculated with the dispersion relation (51), are shown; different lengths are considered, the boundary conditions are periodic, j is the number of half waves along the CNT axis and $n = 2$ denotes the number of nodal diameters. From this figure, it is confirmed that the natural frequency of a vibrational mode (j, n) increases with the number of longitudinal half waves and decreases with increasing length.

It is significant to compare the results of the dispersion relation (51), from the reduced Sanders-Koiter theory (RSKT), with those corresponding to the exact solution (Equation 1.120 of Ref. [38]). This may be seen in Figure 3 and Table 6. From the comparisons, it may be observed that the exact solution and the RSKT are in good agreement in the case of a small number of half waves along the CNT axis ($j \leq 3$), when the ring and tangential shear deformation effects are small. On the other hand, the difference increases with j.

In Figure 4 and Table 7, the dependence of the eigenfrequencies of the first four modes on the ratio ($\alpha = R / L$) of a CNT having (r, s) = (10, 0) is shown; the eigenfrequencies decrease as the CNT length increases. In the limit $\alpha \rightarrow 0$, the eigenfrequency is the same for any wave number j, because it corresponds to the eigenfrequency of a thin circular ring, in the following form [44]

$$\omega = \frac{n(n^2-1)}{\sqrt{12(n^2+1)}}\beta \tag{66}$$

5.3. Comparison between the models

In this section, the analytical and numerical models, based on the reduced Sanders-Koiter theory (RSKT) and the complete Sanders-Koiter theory (CSKT), are compared.

RSKT can be applied to the calculation of the eigenfrequencies of CNT vibrations with "angular vibration number" $n \geq 2$ [44]. The approximations of the RSKT with respect to the CSKT take into account the relative smallness of the bending and torsion stiffness with respect to those of tension and shear. This involves a correct description of long-wave modes: the range of RSKT applicability can be extended for an increased length of CNT.

The results of the RSKT and the CSKT for different lengths and boundary conditions of a (10, 0) SWNT are shown in Tables 8-9 and Figures 5-8. From the comparisons, it can be firstly noted that the differences between RSKT and CSKT are significant for short CNTs in a large range of

longitudinal waveform numbers j, as expected. Indeed, in this case the effect of the circumferential and tangential shear deformations is not negligible. Furthermore, when the length of the CNT increases, differences between RSKT and CSKT decrease, because the influence of the boundary conditions on the natural frequencies reduces.

In Figure 9, the first six mode shapes of a (r = 10, s = 0, χ = 12.8) SWNT with free edges for the circumferential wavenumber (n = 2) are reported. These mode shapes are obtained by using the equivalent parameters (h, E, ν, ρ) of Table 1. The modes (j = 0, n = 2) and (j = 1, n = 2) correspond to the Rayleigh's inextensional symmetric mode (uniform vibration) and Love's asymmetric mode (one-half of the wave length), respectively (Ref. [38]). The modes (j = 2, n = 2) (wave length) and (j = 4, n = 2) are symmetric, the modes (j = 3, n = 2) and (j = 5, n = 2) are asymmetric, with respect to the central transversal section of the CNT. Such graphical representation of modes could be useful for interpreting the previous results and comparisons.

6. Conclusions

In this paper, a comprehensive analysis of the vibration spectrum of Single-Walled Carbon Nanotubes in the framework of the continuum shell theory is presented.

Size effects are neglected because the present paper is focused on low frequencies of SWNTs with large aspect ratios and diameters.

Significant results concerning applicability, experimental verification and possibility of analytical study for the most important boundary conditions are presented.

1. The results obtained from a numerical model based on the Sanders-Koiter shell theory, which does not introduce any restriction on the geometric parameters and wave numbers, are in excellent agreement with the existing experimental and molecular dynamics data.

→ a. The theory is accurate for SWNTs having large aspect ratios and diameters.

2. An analytical model based on a reduced version of the Sanders-Koiter shell theory is presented. It supplies a new tool valid in a wide parameter range, where other simpler elastic shell theories (e.g., Donnell shallow shell or semi-momentless theories) are not accurate.

→ a. The analytical model gives results close to those from the numerical model for low-frequency normal vibrations.

→ b. The possibility of having an efficient analytical solution allows the spatial structure of normal modes to be clarified: in particular, it reveals the edge effects and their prolongation, which are dependent on the geometric parameters and wave numbers.

Starting from the two models presented here, a future work will consider the energy distribution on the carbon nanotube in nonlinear field, including the presence of conjugate modes, which can give rise to travelling-wave response moving along the circumferential direction of the CNT.

References

[1] Iijima S. Helical microtubules of graphitic carbon. *Nature* 354 (1991) 56-58.

[2] Rao AM, Richter E, Bandow S, Chase B, Eklund PC, Williams KA, Fang S, Subbaswamy KR, Menon M, Thess A, Smalley RE, Dresselhaus G, Dresselhaus MS. Diameter-Selective Raman Scattering from Vibrational Modes in Carbon Nanotubes. *Science* 275 (1997) 187-191.

[3] Bandow S, Asaka S, Saito Y, Rao AM, Grigorian L, Richter E, Eklund PC. Effect of the Growth Temperature on the Diameter Distribution and Chirality of Single-Wall Carbon Nanotubes. *Physical Review Letters* 80(17) (1998) 3779-3782.

[4] Jorio A, Saito R, Hafner JH, Lieber CM, Hunter M, McClure T, Dresselhaus G, Dresselhaus MS. Structural (n,m) Determination of Isolated Single-Wall Carbon Nanotubes by Resonant Raman Scattering. *Physical Review Letters* 86(6) (2001) 1118-1121.

[5] Gupta SS, Bosco FG, Batra RC. Breakdown of structural models for vibrations of single-wall zigzag carbon nanotubes. *Journal of Applied Physics* 106 (2009) 063527(9).

[6] Cheng HC, Liu YL, Wu CH, Chen WH. On radial breathing vibration of carbon nanotubes. *Computational Methods in Applied Mechanical Engineering* 199 (2010) 2820-2827.

[7] Gupta SS, Bosco FG, Batra RC. Wall thickness and elastic moduli of single-walled carbon nanotubes from frequencies of axial, torsional and inextensional modes of vibration. *Computational Materials Science* 47 (2010) 1049-1059.

[8] Duan WH, Wang CM, Zhang YY. Calibration of nonlocal scaling effect parameter for free vibration of carbon nanotubes by molecular dynamics. *Journal of Applied Physics* 101 (2007) 024305(7).

[9] Sakhaee-Pour A, Ahmadian MT, Vafai A. Vibration analysis of single-walled carbon nanotubes using beam element. *Thin-Walled Structures* 47 (2009) 646-652.

[10] Arghavan S, Singh AV. On the vibrations of single-walled carbon nanotubes. *Journal of Sound and Vibration* 330 (2011) 3102-3122.

[11] Odegard GM, Gates TS, Nicholson LM, Wise KE. Equivalent-Continuum Modeling of Nano-Structured Materials. *Composites Science and Technology* 62(14) (2002) 1869-1880.

[12] Lu P, Lee HP, Lu C, Zhang PQ. Application of nonlocal beam models for carbon nanotubes. *International Journal of Solids and Structures* 44 (2007) 5289-5300.

[13] Yang S, Yu S, Kyoung W, Han DS, Cho M. Multiscale modeling of size-dependent elastic properties of carbon nanotube/polymer nanocomposites with interfacial imperfections. *Polymer* 53 (2012) 623-633.

[14] Kiani K. A meshless approach for free transverse vibration of embedded single-walled nanotubes with arbitrary boundary conditions accounting for nonlocal effect. *International Journal of Mechanical Sciences* 52(10) (2010) 1343-1356.

[15] Kiani K. Application of nonlocal beam models to double-walled carbon nanotubes under a moving nanoparticle. Part I: theoretical formulations. *Acta Mechanica* 216 (1-4) (2011) 165-195.

[16] Kiani K. Application of nonlocal beam models to double-walled carbon nanotubes under a moving nanoparticle. Part II: parametric study. *Acta Mechanica* 216 (1-4) (2011) 197-206.

[17] Kiani K. Vibration analysis of elastically restrained double-walled carbon nanotubes on elastic foundation subjected to axial load using nonlocal shear deformable beam theories. *International Journal of Mechanical Sciences* 68 (2013) 16-34.

[18] Kiani K. Vibration behavior of simply supported inclined single-walled carbon nanotubes conveying viscous fluids flow using nonlocal Rayleigh beam model. *Applied Mathematical Modelling* 37(4) (2013) 1836-1850.

[19] Wang L, Hu H. Flexural wave propagation in single-walled carbon nanotubes. *Physical Review B* 71 (2005) 195412(7).

[20] Fazelzadeh SA, Ghavanloo E. Nonlocal anisotropic elastic shell model for vibrations of single-walled carbon nanotubes with arbitrary chirality. *Composite Structures* 94 (2012) 1016-1022.

[21] Ru CQ. Axially compressed buckling of a doublewalled carbon nanotube embedded in an elastic medium. *Journal of the Mechanics and Physics of Solids* 49 (2001) 1265-1279.

[22] He XQ, Eisenberger M, Liew KM. The effect of Van der Waals interaction modeling on the vibration characteristics of multiwalled carbon nanotubes. *Journal of Applied Physics* 100 (2006) 124317(12).

[23] Elishakoff I, Pentaras D. Fundamental natural frequencies of double-walled carbon nanotubes. *Journal of Sound and Vibration* 322 (2009) 652-664.

[24] Silvestre N, Wang CM, Zhang YY, Xiang Y. Sanders shell model for buckling of single-walled carbon nanotubes with small aspect ratio. *Composite Structures* 93 (2011) 1683-1691.

[25] Peng J, Wu J, Hwang KC, Song J, Huang Y. Can a Single-Wall Carbon Nanotube Be Modeled as a Thin Shell? *Journal of the Mechanics and Physics of Solids* 56 (2008) 2213-2224.

[26] Huang Y, Wu J, Hwang KC. Thickness of graphene and single-wall carbon nanotubes. *Physical Review B* 74 (2006) 245413(9).

[27] Yao N, Lordi V. Young's modulus of single-walled carbon nanotubes. *Journal of Applied Physics* 84(4) (1998) 1939-1943.

[28] Yakobson BI, Brabec CJ, Bernholc J. Nanomechanics of Carbon Tubes: Instabilities beyond Linear Response. *Physical Review Letters* 76(14) (1996) 2511-2514.

[29] Jin Y, Yuan FG. Simulation of elastic properties of single-walled carbon nanotubes. *Composite Science and Technology* 63 (2003) 1507-1515.

[30] Vodenitcharova T, Zhang LC. Effective wall thickness of a single-walled carbon nanotube. *Physical Review B* 68 (2003) 165401(4).

[31] Liew KM, Wang Q. Analysis of wave propagation in carbon nanotubes via elastic shell theories. *International Journal of Engineering Science* 45 (2007) 227-241.

[32] Brischetto S, Carrera E. Classical and refined shell models for the analysis of nano-reinforced structures. *International Journal of Mechanical Sciences* 55 (2012) 104-117.

[33] Silvestre N. On the accuracy of shell models for torsional buckling of carbon nanotubes. *European Journal of Mechanics A/Solids* 32 (2012) 103-108.

[34] Wang CY, Ru CQ, Mioduchowski A. Applicability and Limitations of Simplified Elastic Shell Equations for Carbon Nanotubes. *Journal of Applied Mechanics* 71 (2004) 622-631.

[35] Cong W. Modeling and Analysis of Carbon Nanotube Buckling Using Thick Shell Theory. *Engineering Science Programme*, National University of Singapore, 2011.

[36] Ghavanloo E, Fazelzadeh SA. Vibration characteristics of single-walled carbon nanotubes based on an anisotropic elastic shell model including chirality effect. *Applied Mathematical Modelling* 36(10) (2012) 4988-5000.

[37] Chang T. A molecular based anisotropic shell model for single-walled carbon nanotubes. *Journal of the Mechanics and Physics of Solids* 58 (2010) 1422-1433.

[38] Leissa AW. *Vibrations of Shells*. Government Printing Office, Washington DC, 1973.

[39] Yamaki N. *Elastic Stability of Circular Cylindrical Shells*. North-Holland, Amsterdam, 1984.

[40] Amabili M. *Nonlinear Vibrations and Stability of Shells and Plates* (2008). Cambridge University Press. New York.

[41] Pellicano F. Vibrations of circular cylindrical shells: Theory and experiments. *Journal of Sound and Vibration* 303 (2007) 154-170.

[42] Pellicano F. Dynamic instability of a circular cylindrical shell carrying a top mass under base excitation: Experiments and theory. *International Journal of Solids and Structures* 48 (2011) 408-427.

[43] Strozzi M, Pellicano F. Nonlinear vibrations of functionally graded cylindrical shells. *Thin-Walled Structures* 67 (2013) 63-77.

[44] Smirnov VV, Shepelev DS, Manevitch LI. Localization of bending vibrations in the Single-Walled Carbon Nanotubes. *Nanosystems: Physics, Chemistry, Mathematics* 2(2) (2011) 102-106.

List of table captions

Table 1. Effective and equivalent parameters of the Single-Walled Carbon Nanotubes [28].

Table 2. Natural frequencies of the radial breathing mode ($j = 0$, $n = 0$): comparisons between the complete Sanders-Koiter theory (CSKT) and the Resonant Raman Spectroscopy (RRS).

Table 3. Natural frequencies of the radial breathing mode ($j = 0$, $n = 0$): comparisons between the complete Sanders-Koiter theory (CSKT) and the Molecular Dynamics Simulations (MDS).

Table 4. Natural frequencies of the beam-like modes ($n = 1$): comparisons between the complete Sanders-Koiter theory (CSKT) and the Molecular Dynamics Simulations (MDS).

Table 5. Natural frequencies of the beam-like modes ($n = 1$): comparisons between the complete Sanders-Koiter theory (CSKT) and the Finite Element Analyses (FEA).

Table 6. Natural frequencies (THz) of the SWNT ($L = 6.0$ nm): comparisons between the exact solution of the equations of motion (Eq. (1.120), Ref. [38]) and the reduced Sanders-Koiter theory (RSKT) (Eq. (51)).

Table 7. Dependence of the eigenfrequencies of the first four modes on the ratio ($\alpha = R / L$) of the (r, s) = (10, 0) CNT for the reduced Sanders-Koiter theory (RSKT) (Eq. (51)) with periodic boundary conditions.

Table 8. Natural frequencies of the Single-Walled Carbon Nanotubes ($L = 3.0$ nm) and ($L = 10.0$ nm) with free edges: comparisons between the complete (CSKT) and reduced (RSKT) Sanders-Koiter theories.

Table 9. Natural frequencies of the Single-Walled Carbon Nanotubes ($L = 3.0$ nm) and ($L = 10.0$ nm) with clamped edges: comparisons between the complete (CSKT) and reduced (RSKT) Sanders-Koiter theories.

Effective thickness h_0 (nm)	0.10 ÷ 0.15
Equivalent thickness h (nm)	0.066
Effective Young's modulus E_0 (TPa)	1.0 ÷ 2.0
Equivalent Young's modulus E (TPa)	5.5
Effective Poisson's ratio v_0	0.12 ÷ 0.28
Equivalent Poisson's ratio v	0.19
Surface density of graphite σ (kg/m^2)	7.718×10^{-7}
Equivalent mass density ρ (kg/m^3)	11700

Table 1. Effective and equivalent parameters of the Single-Walled Carbon Nanotubes [28].

Natural frequency (THz)			Difference %
(*r*, *s*)	CSKT – Present model	RRS – Ref. [4]	
(8, 7)	6.905	7.165	3.63
(10, 5)	6.785	7.105	4.50
(11, 4)	6.669	6.865	2.85
(14, 1)	6.177	6.295	1.87
(18, 0)	5.025	5.276	4.76
(17, 2)	4.964	5.216	4.83
(16, 4)	4.895	5.066	3.37
(15, 6)	4.788	4.947	3.21
(11, 11)	4.711	4.917	4.19
(19, 1)	4.594	4.797	4.23
(18, 3)	4.559	4.737	3.76
(13, 10)	4.494	4.677	3.91
(17, 5)	4.494	4.677	3.91
(16, 7)	4.393	4.617	4.85
(12, 12)	4.318	4.527	4.62
(21, 0)	4.271	4.437	3.74
(18, 6)	4.150	4.317	4.04

Table 2. Natural frequencies of the radial breathing mode ($j = 0$, $n = 0$): comparisons between the complete Sanders-Koiter theory (CSKT) and the Resonant Raman Spectroscopy (RRS).

Natural frequency (THz)			Difference %
(*r*, *s*)	CSKT – Present model	MDS – Ref. [7]	
(10, 0)	8.966	8.718	2.84
(6, 6)	8.636	8.348	3.45
(12, 0)	7.478	7.272	2.83
(7, 7)	7.399	7.166	3.25
(8, 8)	6.473	6.275	3.15
(14, 0)	6.414	6.235	2.87
(16, 0)	5.606	5.455	2.77
(10, 10)	5.184	5.026	3.14
(18, 0)	4.985	4.850	2.78
(20, 0)	4.489	4.364	2.86
(12, 12)	4.318	4.190	3.05
(25, 0)	3.590	3.491	2.84
(15, 15)	3.453	3.354	2.95
(30, 0)	2.991	2.908	2.85
(18, 18)	2.878	2.796	2.93
(33, 0)	2.718	2.623	3.62
(20, 20)	2.590	2.516	2.94

Table 3. Natural frequencies of the radial breathing mode ($j = 0$, $n = 0$): comparisons between the complete Sanders-Koiter theory (CSKT) and the Molecular Dynamics Simulations (MDS).

Natural frequency (THz)			Difference %
$(r, s) = (5, 5)$	$\chi = 5.26$		
Clamped – Free CF			
(j, n)	CSKT – Present model	MDS – Ref. [8]	
(0, 1)	0.217	0.212	2.36
(1, 1)	1.071	1.043	2.68
(2, 1)	2.411	2.340	3.03
(3, 1)	3.800	3.682	3.20
Clamped – Clamped CC			
(j, n)	CSKT – Present model	MDS – Ref. [8]	
(1, 1)	1.018	0.975	4.41
(2, 1)	2.192	2.105	4.13
(3, 1)	3.529	3.404	3.67
(4, 1)	4.858	4.724	2.84
$(r, s) = (5, 5)$	$\chi = 10.34$		
Clamped – Free CF			
(j, n)	CSKT – Present model	MDS – Ref. [8]	
(0, 1)	0.058	0.060	3.33
(1, 1)	0.338	0.344	1.74
(2, 1)	0.856	0.864	0.93
(3, 1)	1.494	1.499	0.33
Clamped – Clamped CC			
(j, n)	CSKT – Present model	MDS – Ref. [8]	
(1, 1)	0.335	0.336	0.30
(2, 1)	0.819	0.818	0.12
(3, 1)	1.428	1.417	0.78
(4, 1)	2.095	2.079	0.77

Table 4. Natural frequencies of the beam-like modes ($n = 1$): comparisons between the complete Sanders-Koiter theory (CSKT) and the Molecular Dynamics Simulations (MDS).

Natural frequency (THz)			Difference %
$(r, s) = (8, 0)$	$\chi = 24.29$		
Clamped – Free CF			
(j, n)	CSKT – Present model	FEA – Ref. [9]	
(0, 1)	0.011	0.011	0.00
(1, 1)	0.072	0.068	5.88
(2, 1)	0.196	0.185	5.94
(3, 1)	0.372	0.354	5.08
Clamped – Clamped CC			
(j, n)	CSKT – Present model	FEA – Ref. [9]	
(1, 1)	0.072	0.069	4.35
(2, 1)	0.194	0.186	4.30
(3, 1)	0.368	0.354	3.95
(4, 1)	0.583	0.565	3.19
$(r, s) = (20, 0)$	$\chi = 19.60$		
Clamped – Free CF			
(j, n)	CSKT – Present model	FEA – Ref. [9]	
(0, 1)	0.007	0.007	0.00
(1, 1)	0.043	0.043	0.00
(2, 1)	0.118	0.117	0.85
(3, 1)	0.220	0.220	0.00
Clamped – Clamped CC			
(j, n)	CSKT – Present model	FEA – Ref. [9]	
(1, 1)	0.044	0.044	0.00
(2, 1)	0.116	0.116	0.00
(3, 1)	0.216	0.217	0.46
(4, 1)	0.338	0.340	0.59

Table 5. Natural frequencies of the beam-like modes ($n = 1$): comparisons between the complete Sanders-Koiter theory (CSKT) and the Finite Element Analyses (FEA).

Natural frequency (THz)			Difference %
$(r, s) = (10, 0)$		$\chi = 7.66$	
(j, n)	Exact solution (Eq. (1.120), Ref. [38])	RSKT (Eq. (51))	
(0, 2)	1.14749	1.17233	2.12
(1, 2)	1.16069	1.18721	2.23
(2, 2)	1.23115	1.26565	2.73
(3, 2)	1.41766	1.48565	4.58
(4, 2)	1.74250	1.90633	8.59
(5, 2)	2.17980	2.53387	14.0
(6, 2)	2.69010	3.34718	19.6

Table 6. Natural frequencies (THz) of the SWNT (L = 6.0 nm): comparisons between the exact solution of the equations of motion (Eq. (1.120), Ref. [38]) and the reduced Sanders-Koiter theory (RSKT) (Eq. (51)).

$(r, s) = (10, 0)$		Natural frequency (THz)			
L (nm)	$\alpha = R / L$	$j = 1$	$j = 2$	$j = 3$	$j = 4$
7.80	0.05019	1.17602	1.20963	1.29762	1.46452
7.41	0.05283	1.17693	1.21580	1.31833	1.51060
7.02	0.05577	1.17802	1.22341	1.34377	1.56614
6.63	0.05905	1.17936	1.23292	1.37530	1.63345
6.24	0.06274	1.18101	1.24495	1.41474	1.71547
5.85	0.06692	1.18309	1.26042	1.46452	1.81592
5.46	0.07170	1.18575	1.28062	1.52796	1.93962
5.07	0.07722	1.18923	1.30745	1.60954	2.09278
4.68	0.08365	1.19391	1.34377	1.71547	2.28352
4.29	0.09126	1.20038	1.39390	1.85430	2.52258
3.90	0.10038	1.20963	1.46452	2.03800	2.82435
3.51	0.11154	1.22341	1.56614	2.28352	3.20852
3.12	0.12548	1.24495	1.71547	2.61536	3.70280
2.73	0.14341	1.28062	1.93962	3.06980	4.34777
2.34	0.16731	1.34377	2.28352	3.70280	5.20730
1.95	0.20077	1.46452	2.82435	4.60626	6.39689
1.56	0.25096	1.71547	3.70280	5.95247	8.18521

Table 7. Dependence of the eigenfrequencies of the first four modes on the ratio ($\alpha = R / L$) of the (r, s) = (10, 0) CNT for the reduced Sanders-Koiter theory (RSKT) (Eq. (51)) with periodic boundary conditions.

Natural frequency (THz)			Difference %
$(r, s) = (10, 0)$		$\chi = 3.83$	
(j, n)	CSKT	RSKT	
(0, 2)	1.18809	1.17233	1.34
(1, 2)	1.21558	1.28695	5.55
(2, 2)	1.52195	1.79994	15.4
(3, 2)	2.32386	2.75450	15.6
(4, 2)	3.43668	4.21802	18.5
(5, 2)	4.63191	6.13461	24.5
$(r, s) = (10, 0)$		$\chi = 12.8$	
(j, n)	CSKT	RSKT	
(0, 2)	1.17397	1.17233	0.14
(1, 2)	1.17633	1.17857	0.19
(2, 2)	1.19469	1.20186	0.60
(3, 2)	1.22705	1.25319	2.09
(4, 2)	1.29110	1.34579	4.06
(5, 2)	1.39923	1.49071	6.14

Table 8. Natural frequencies of the Single-Walled Carbon Nanotubes (L = 3.0 nm) and (L = 10.0 nm) with free edges: comparisons between the complete (CSKT) and reduced (RSKT) Sanders-Koiter theories.

Natural frequency (THz)			Difference %
(r, s) = (10, 0)		χ = 3.83	
(j, n)	CSKT	RSKT	
(1, 2)	1.38791	1.42490	2.60
(2, 2)	2.04764	2.51265	18.5
(3, 2)	3.02770	4.32504	30.0
(4, 2)	4.14980	6.73340	38.4
(5, 2)	5.32216	9.59525	44.5
(r, s) = (10, 0)		χ = 12.8	
(j, n)	CSKT	RSKT	
(1, 2)	1.17628	1.17947	0.27
(2, 2)	1.20309	1.20720	0.34
(3, 2)	1.26423	1.27119	0.55
(4, 2)	1.36249	1.39041	2.01
(5, 2)	1.51007	1.57960	4.40

Table 9. Natural frequencies of the Single-Walled Carbon Nanotubes (L = 3.0 nm) and (L = 10.0 nm) with clamped edges: comparisons between the complete (CSKT) and reduced (RSKT) Sanders-Koiter theories.

List of figure captions

Figure 1. Geometry of the circular cylindrical shell. (a) Complete shell; (b) cross-section of the shell surface.

Figure 2. Eigenfrequencies of the first modes for the zigzag (10, 0) SWNT. Reduced Sanders-Koiter theory (Eq. (51)). Periodic boundary conditions. $n = 2$. "-♦-", $L = 3.0$ nm; "-■-", $L = 6.0$ nm; "-▲-", $L = 10.0$.

Figure 3. Dispersion curves for the zigzag (10, 0) SWNT. $L = 6.0$ nm. $n = 2$. "-♦-", exact solution of (Eq. (1.120), Ref. [38]); "-■-", reduced Sanders-Koiter theory (Eq. (51)).

Figure 4. Dependence of the eigenfrequencies on the ratio ($\alpha = R / L$). Zigzag (10, 0) SWNT. Reduced Sanders-Koiter theory (Eq. (51)). Periodic boundary conditions. $n = 2$. "-♦-", $j = 1$; "-■-", $j = 2$; "-▲-", $j = 3$; "-x-", $j = 4$.

Figure 5. Natural frequencies of the zigzag (10, 0) SWNT. $L = 3.0$ nm. $n = 2$. Free edges. "-♦-", complete Sanders-Koiter theory (CSKT); "-■-", reduced Sanders-Koiter theory (RSKT).

Figure 6. Natural frequencies of the zigzag (10, 0) SWNT. $L = 10.0$ nm. $n = 2$. Free edges. "-♦-", complete Sanders-Koiter theory (CSKT); "-■-", reduced Sanders-Koiter theory (RSKT).

Figure 7. Natural frequencies of the zigzag (10, 0) SWNT. $L = 3.0$ nm. $n = 2$. Clamped edges. "-♦-", complete Sanders-Koiter theory (CSKT); "-■-", reduced Sanders-Koiter theory (RSKT).

Figure 8. Natural frequencies of the zigzag (10, 0) SWNT. $L = 10.0$ nm. $n = 2$. Clamped edges. "-♦-", complete Sanders-Koiter theory (CSKT); "-■-", reduced Sanders-Koiter theory (RSKT).

Figure 9. Mode shapes of the SWNT ($r = 10$, $s = 0$, $L = 10.0$ nm); equivalent parameters of Table 1; free edges. a) ($j = 0$, $n = 2$). b) ($j = 1$, $n = 2$). c) ($j = 2$, $n = 2$). d) ($j = 3$, $n = 2$). e) ($j = 4$, $n = 2$). f) ($j = 5$, $n = 2$).

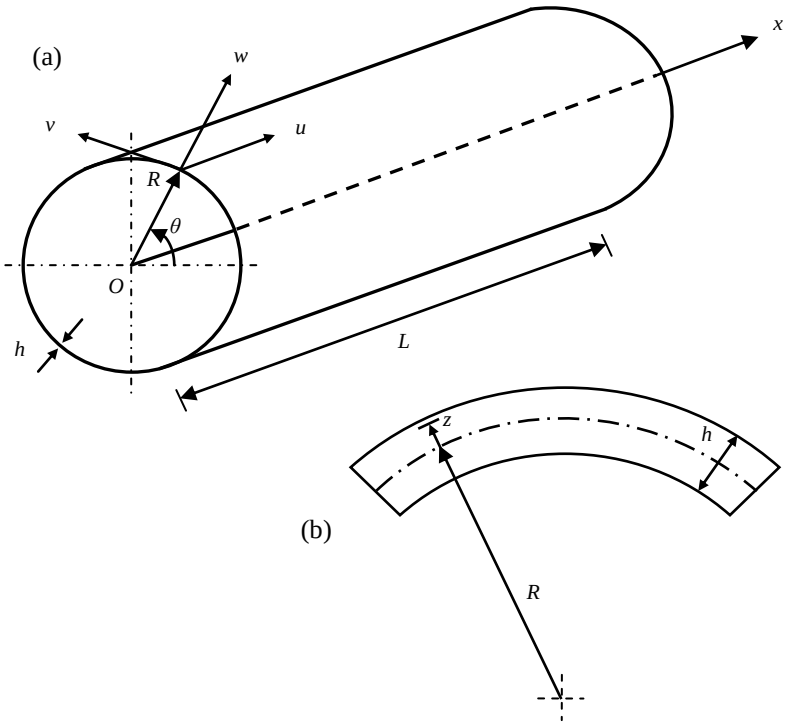

Figure 1. Geometry of the circular cylindrical shell.
(a) Complete shell; (b) cross-section of the shell surface.

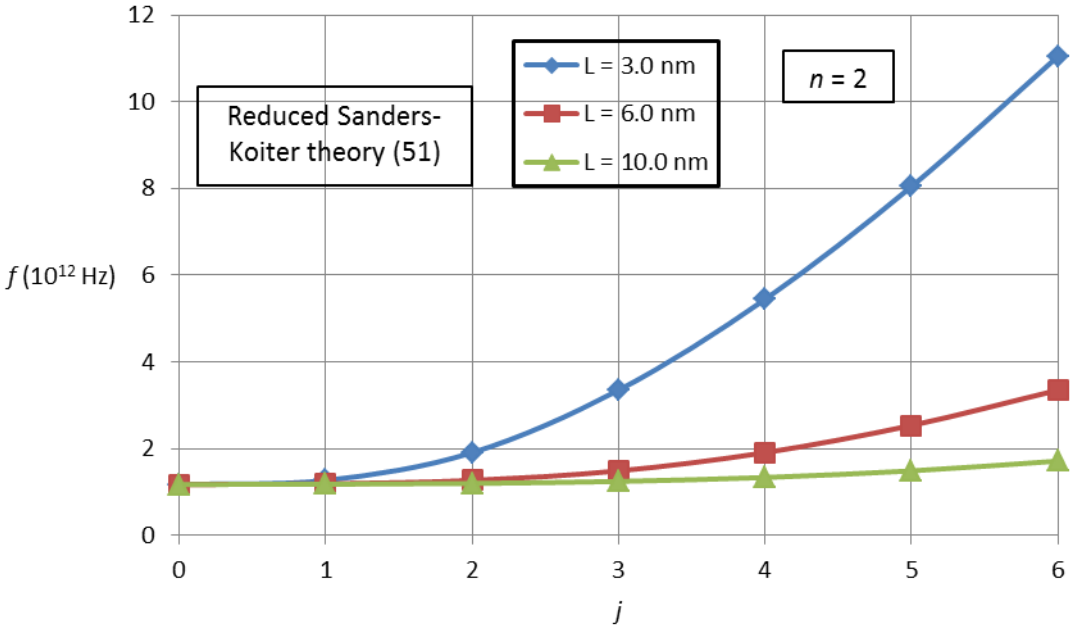

Figure 2. Eigenfrequencies of the first modes for the zigzag (10, 0) SWNT. Reduced Sanders-Koiter theory (Eq. (51)). Periodic boundary conditions. $n = 2$. "-♦-", $L = 3.0$ nm; "-■-", $L = 6.0$ nm; "-▲-", $L = 10.0$ nm.

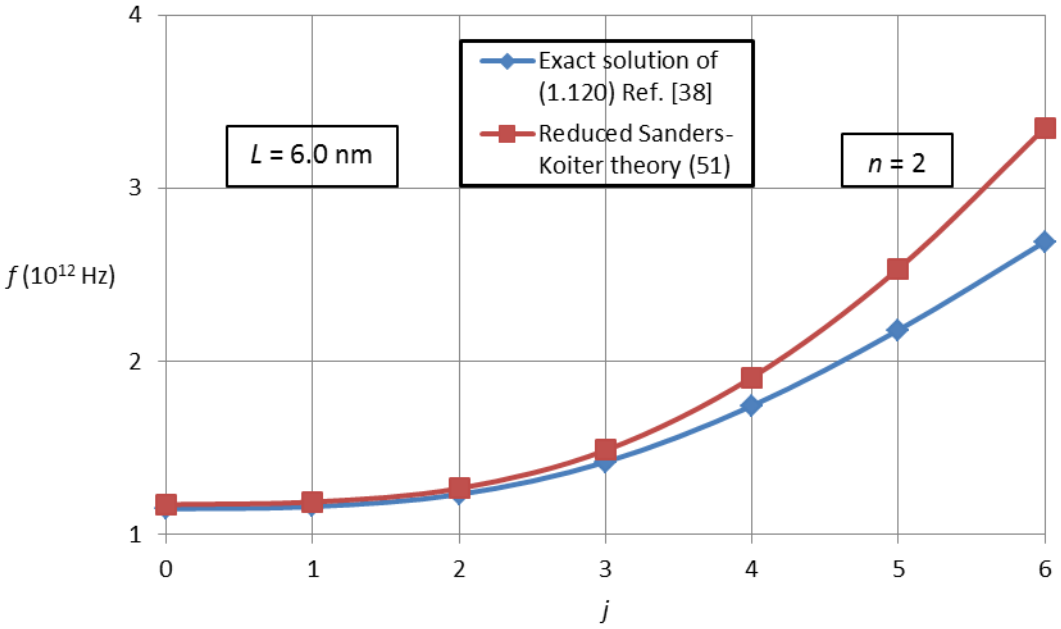

Figure 3. Dispersion curves for the zigzag (10, 0) SWNT. L = 6.0 nm. n = 2. "-♦-", exact solution of (Eq. (1.120), Ref. [38]); "-■-", reduced Sanders-Koiter theory (Eq. (51)).

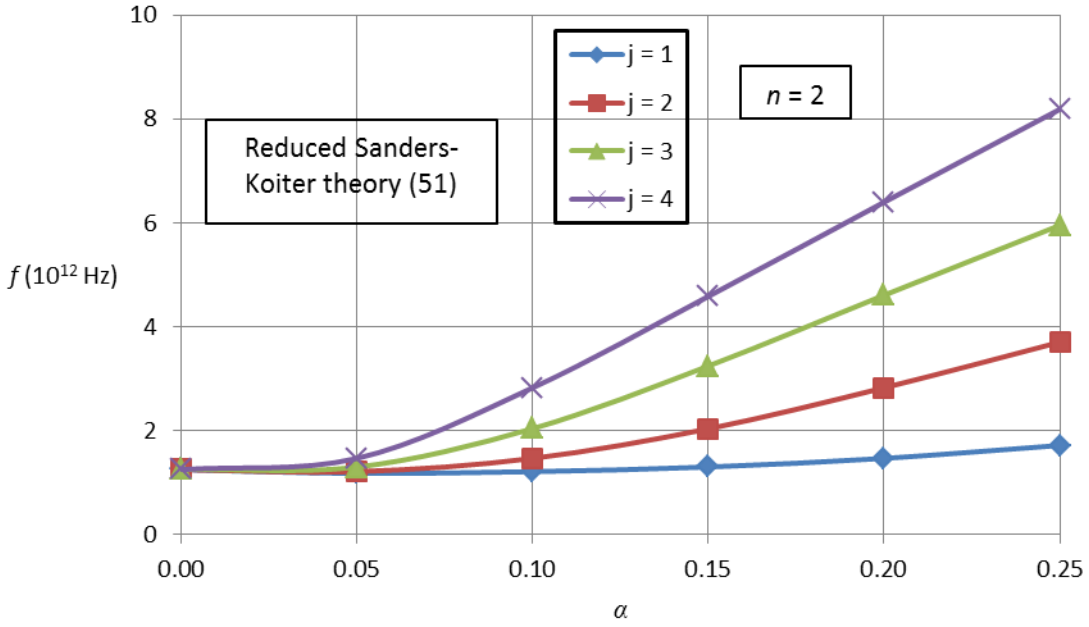

Figure 4. Dependence of the eigenfrequencies on the ratio ($\alpha = R / L$). Zigzag (10, 0) SWNT. Reduced Sanders-Koiter theory (Eq. (51)). Periodic boundary conditions. $n = 2$. "-♦-", $j = 1$; "-■-", $j = 2$; "-▲-", $j = 3$; "-x-", $j = 4$.

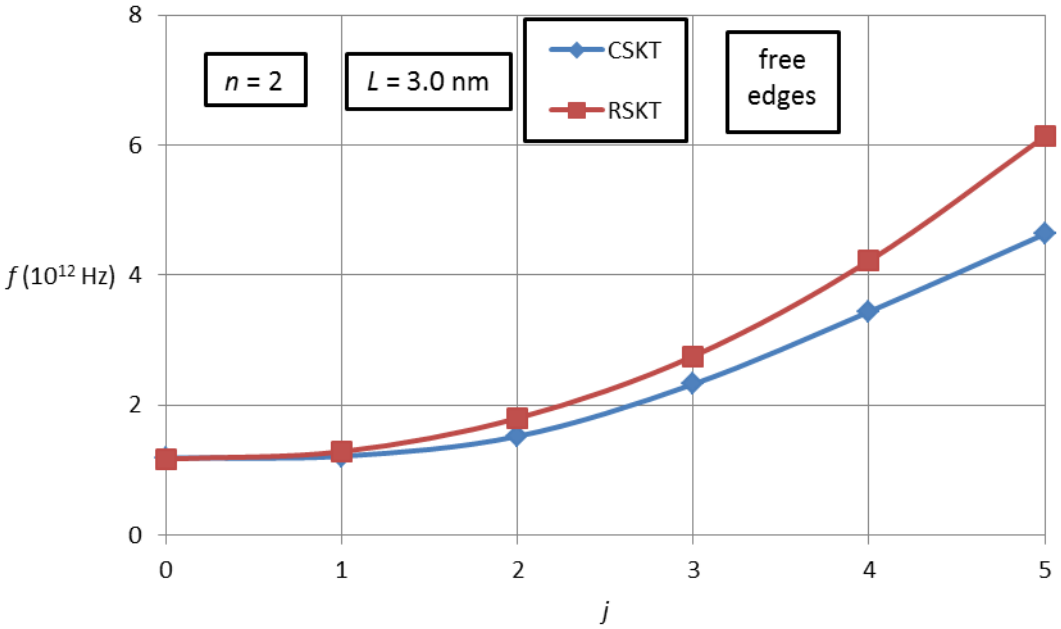

Figure 5. Natural frequencies of the zigzag (10, 0) SWNT. L = 3.0 nm. n = 2. Free edges. "-♦-", complete Sanders-Koiter theory (CSKT); "-■-", reduced Sanders-Koiter theory (RSKT).

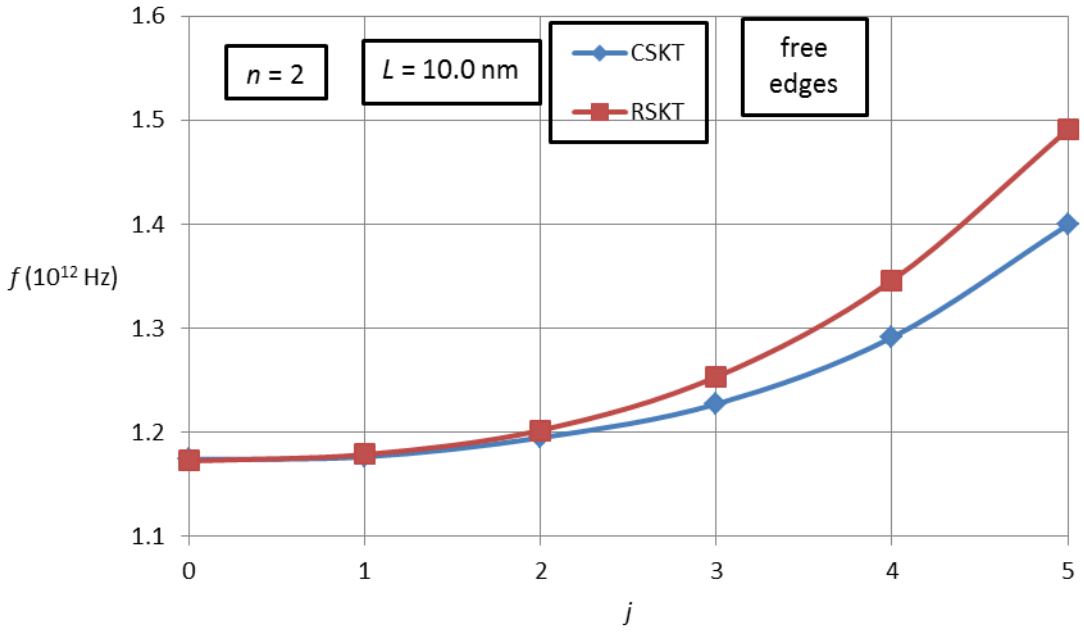

Figure 6. Natural frequencies of the zigzag (10, 0) SWNT. L = 10.0 nm. n = 2. Free edges. "-♦-", complete Sanders-Koiter theory (CSKT); "-■-", reduced Sanders-Koiter theory (RSKT).

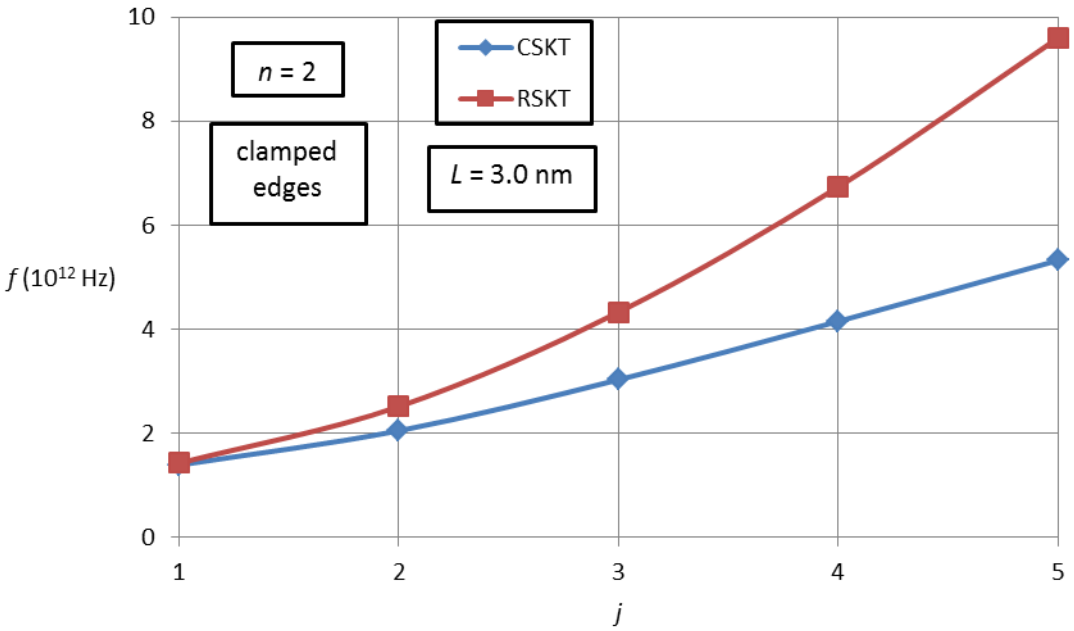

Figure 7. Natural frequencies of the zigzag (10, 0) SWNT. L = 3.0 nm. n = 2. Clamped edges. "-♦-", complete Sanders-Koiter theory (CSKT); "-■-", reduced Sanders-Koiter theory (RSKT).

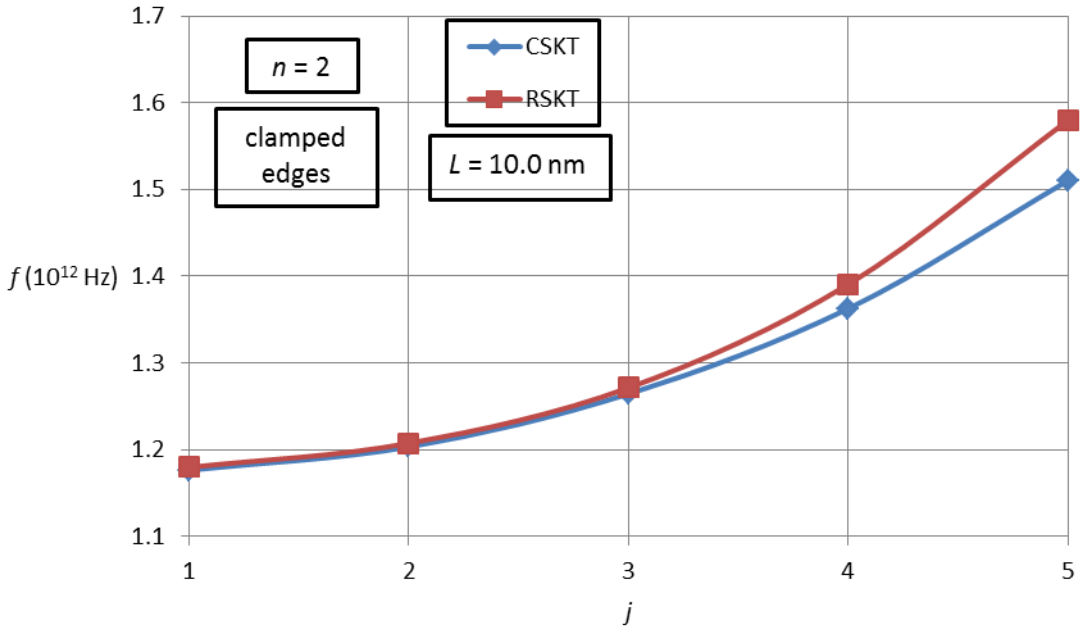

Figure 8. Natural frequencies of the zigzag (10, 0) SWNT. L = 10.0 nm. n = 2. Clamped edges. "-♦-", complete Sanders-Koiter theory (CSKT); "-■-", reduced Sanders-Koiter theory (RSKT).

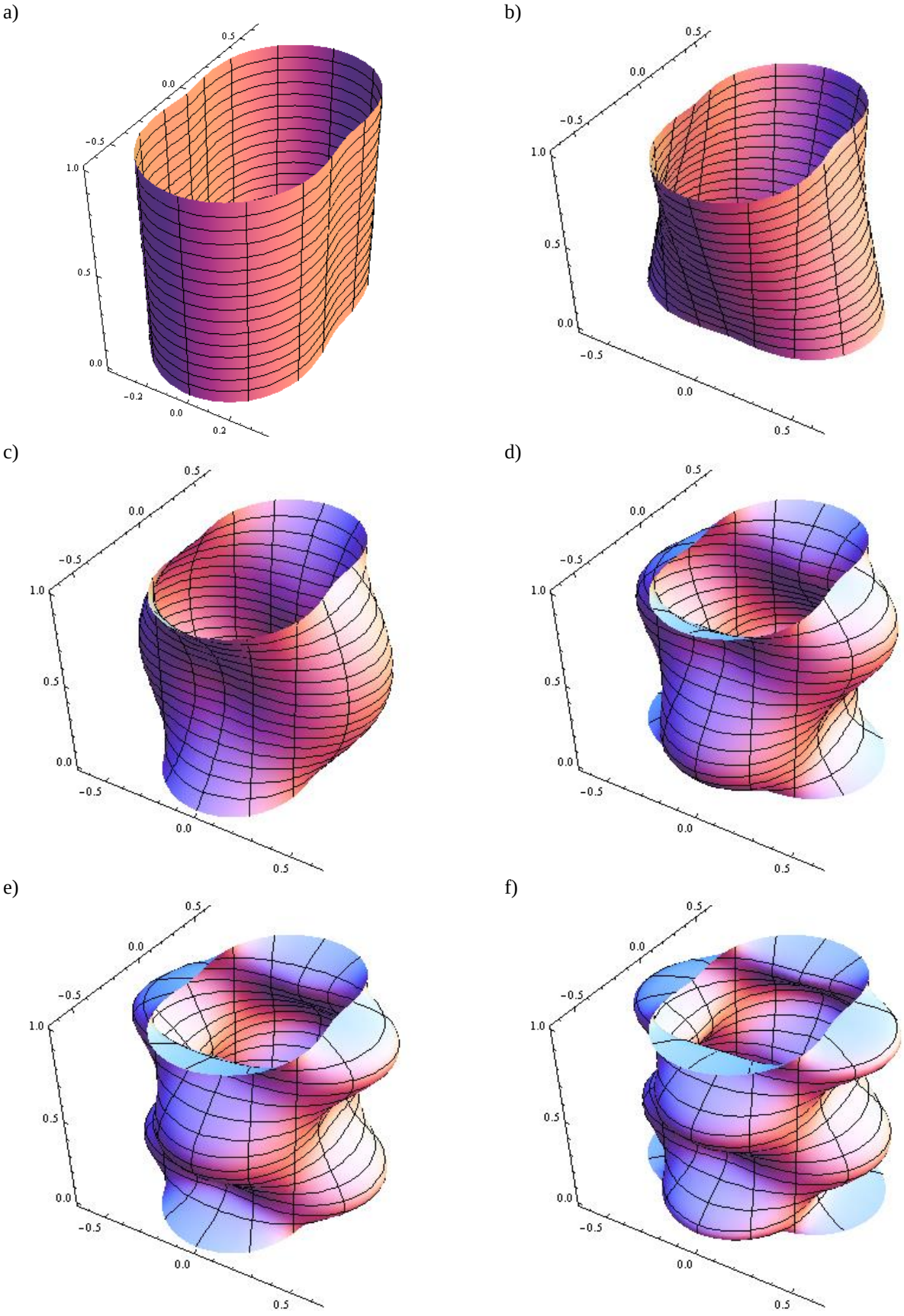

Figure 9. Mode shapes of the SWNT (r = 10, s = 0, L = 10.0 nm); equivalent parameters of Table 1; free edges. a) (j = 0, n = 2). b) (j = 1, n = 2). c) (j = 2, n = 2). d) (j = 3, n = 2). e) (j = 4, n = 2). f) (j = 5, n = 2).